

LETTER • OPEN ACCESS

## Sustainability of fresh groundwater resources in fifteen major deltas around the world

To cite this article: J van Engelen *et al* 2022 *Environ. Res. Lett.* **17** 125001

View the [article online](#) for updates and enhancements.

You may also like

- [Impacts of 25 years of groundwater extraction on subsidence in the Mekong delta, Vietnam](#)  
P S J Minderhoud, G Erkens, V H Pham et al.
- [Groundwater resources, climate and vulnerability](#)  
C Isabella Bovolo, Geoff Parkin and Marios Sophocleous
- [A model comparison assessing the importance of lateral groundwater flows at the global scale](#)  
Inge E M de Graaf and Kerstin Stahl

ENVIRONMENTAL RESEARCH  
LETTERS

## PAPER

Sustainability of fresh groundwater resources in fifteen major  
deltas around the world

## OPEN ACCESS

## RECEIVED

13 March 2022

## REVISED

30 October 2022

## ACCEPTED FOR PUBLICATION

9 November 2022

## PUBLISHED

18 November 2022

Original Content from  
this work may be used  
under the terms of the  
[Creative Commons  
Attribution 4.0 licence](#).

Any further distribution  
of this work must  
maintain attribution to  
the author(s) and the title  
of the work, journal  
citation and DOI.

J van Engelen<sup>1,\*</sup> , G H P Oude Essink<sup>1,2</sup> and M F P Bierkens<sup>1,2</sup> <sup>1</sup> Unit Subsurface and Groundwater Systems, Deltares, Daltonlaan 600, 3584 BK Utrecht, The Netherlands<sup>2</sup> Department of Physical Geography, Utrecht University, Princetonlaan 10, 3584 BK Utrecht, The Netherlands

\* Author to whom any correspondence should be addressed.

E-mail: [joeri.vanengelen@deltares.nl](mailto:joeri.vanengelen@deltares.nl)

Keywords: groundwater, salinity, deltas, model

## Abstract

Population growth, urbanization and intensification of irrigated agriculture in the world's deltas boost the demand for fresh water, with extensive groundwater extraction as a result. This, in turn, leads to salt water intrusion and upconing, which poses a threat to freshwater and food security. Managing fresh groundwater resources in deltas requires accurate knowledge about the current status and behaviour of their fresh groundwater resources. However, this knowledge is scarcely present, especially for groundwater at larger depths. Here, we use three-dimensional variable-density groundwater model simulations over the last 125 ka to estimate the volume of fresh groundwater resources for 15 major deltas around the world. We estimate current volumes of onshore fresh groundwater resources for individual deltas to vary between  $10^{10}$  m<sup>3</sup> and  $10^{12}$  m<sup>3</sup>. Offshore, the estimated volumes of fresh groundwater are generally smaller, though with a considerably higher variability. In 9 out of 15 simulated deltas, fresh groundwater volumes developed over thousands of years. Based on current groundwater extraction and recharge rates, we estimate the time until *in-situ* fresh groundwater resources are completely exhausted, partly leading to groundwater level decline and mostly replacement with river water or saline groundwater. This straightforward analysis shows that 4 out of 15 deltas risk complete exhaustion of fresh groundwater resources within 300 m depth in 200 years. These deltas also suffer from saline surface water which means their groundwater resources will progressively salinize. With a fourfold increase in extraction rates, seven deltas risk a complete exhaustion within 200 years. Of these seven deltas, six suffer from saline surface water. We stress that the groundwater of these six vulnerable deltas should be carefully managed, to avoid non-renewable groundwater use. The progressive exhaustion of fresh groundwater resources in these deltas will hamper their ability to withstand periods of water scarcity.

## 1. Introduction

River deltas are economic hotspots that are commonly densely populated and harbour lands with high agricultural productivity (Seto 2011, Neumann *et al* 2015). Their growing population in combination with urbanization and intensification of irrigated agriculture are a cause for rising freshwater shortages (Bucx *et al* 2010), which encourages increased groundwater extractions. These, in turn, lead to salt water intrusion and upconing (Werner *et al* 2013, Michael *et al* 2017). Currently, salinization is already affecting many large deltas (Rahman *et al* 2019),

leading to significant agricultural yield loss (Biswas 1993), which in turn decreases regional food security and creates new socio-economic challenges such as migration (Giosan *et al* 2014) and changing farming practices (Smajgl *et al* 2015). Moreover, a relatively high chloride content ( $>500$  mg Cl l<sup>-1</sup>) in drinking water is associated with serious health risks (Khan *et al* 2014, Talukder *et al* 2017, Al Nahian *et al* 2018).

Groundwater management in deltas requires proper knowledge about the current status and behaviour of their fresh groundwater resources. This knowledge, however, is very limited, especially at large depths, which is caused by a lack of observations.

Acquiring better insight into fresh groundwater resources in the world's deltas will pinpoint vulnerable areas and is an essential missing component to include in delta inter-comparison projects, of which several have been accomplished in the last two decades (e.g. Coleman and Huh 2003, Ericson *et al* 2006, Syvitski *et al* 2009, Bucx *et al* 2010, Tessler *et al* 2015, Van Driel *et al* 2015, Wolters and Kuenzer 2015).

Here, we apply three-dimensional variable-density groundwater model simulations spanning the last 125 ka to estimate fresh groundwater volumes of 15 major deltas. For every delta, these volumes are compared to estimates of present-day groundwater extraction rates, to acquire a sense of the deltas' vulnerability to groundwater extraction. The selected deltas differ greatly in size, climate, and population, but face similar issues. For instance, the thick, highly populated Ganges-Brahmaputra delta (India and Bangladesh) dwarfs the thin, scarcely populated Saloum delta (Senegal) in size and population, but both suffer from surface water salinization and are therefore highly depending on groundwater for drinking water and irrigation (Faye *et al* 2005, Ayers *et al* 2016). This work is an advancement of earlier work of the authors (van Engelen *et al* 2020), as site-specific data is used as model input and to validate model results, in order to analyse real world problems, instead of being a pure synthetic study.

## 2. Background: genesis of onshore groundwater salinity in deltas

The present-day groundwater salinity distribution in most deltas presumably developed over thousands of years (Larsen *et al* 2017, van Engelen *et al* 2020), and is often not in a steady state with the groundwater systems' current forcings (Oude Essink 2001). This has been shown with model simulations (Delsman *et al* 2014, Larsen *et al* 2017, Meyer *et al* 2019, Van Pham *et al* 2019, van Engelen *et al* 2019), and is further illustrated by the fact that in many deltas across the globe, zones of saline groundwater are observed far landwards, which have been hypothesized or proven to be caused by a marine transgression (figure 1 and table 1), making this a global phenomenon. Nearly all of these deltas have experienced a marine transgression sometime between 8.5 ka to 6.5 ka (Stanley and Warne 1994), which serves as a reasonable hypothesis to, either fully or partly, explain the inland salinities of most deltas. The only exception to this is the Incomati delta, which did not experience a Holocene transgression but endured several Pleistocene transgressions (Salman and Abdula 1995), of which traces still can be found in its groundwater salinity today (Nogueira *et al* 2019).

Figure 2 sketches a general picture of the evolution of the groundwater salinity distribution. During the last glacial period, the eustatic sea level was significantly lower, up to 125 m (figure 2(a)). This led to

a steep hydraulic gradients and shorelines being located further seawards than nowadays, which in turn exposed a larger area of the continental shelf to natural groundwater recharge, resulting in mostly fresh deltaic aquifers. After this period, sea levels rose rapidly leading to the Holocene transgression (Stanley and Warne 1994), during which sea water infiltrated and consequently the fresh groundwater volumes rapidly declined (figure 2(b)). After the transgression reached its maximum extent, the fresh groundwater volumes partly recovered due to subsequent delta progradation, but not to their level during the Glacial Maximum (figure 2(c)). Finally, humans start to influence the groundwater salinity distribution (figure 2(d)), for example by extracting groundwater and land reclamation projects.

## 3. Methods

### 3.1. Model description

To estimate the present-day volumes of fresh groundwater in 15 major deltas, we used three-dimensional variable-density groundwater models ('paleohydrogeologic models' in short) with which we simulated the last 125 ka, encompassing a full glacial cycle. We applied the paleohydrogeologic models to these 15 deltas with an idealized geometry and lithology. With these models, groundwater salinity distributions were simulated, which aim to approach the present-day groundwater salinity distribution (figure 3). The models were constructed based on a set of 21 inputs, for which an extensive literature study was conducted to find representative values (tables A1 and A2). The inputs with the largest uncertainty and impact on fresh groundwater resources (aquifer horizontal conductivity ( $K_{h, aqt}$ ) and aquitard vertical conductivity ( $K_{v, aqt}$ ), as found previously in van Engelen *et al* 2020) were varied to account for uncertainty. We discretized the input range of  $K_{h, aqt}$  and  $K_{v, aqt}$  in three levels (minimum, logarithmic mean and maximum), and conducted a full factorial analysis for each delta. This resulted in nine simulations per delta.

The planar geometry of the delta was captured with a fan-shape, of which the surface elevation linearly decreased from delta apex to present day coastline. The hydrogeological base was conceptualized as a half-ellipsoid along the radial lines of the fan, with a linear decline in the coastal direction. The deterministic lithology featured a confining layer on top, underneath which a  $N_{aqt}$  number of aquitards was positioned. Each aquitard was incised by a  $N_{pal}$  number of paleochannels. A combination of the eustatic sea level curve (Spratt and Lisiecki 2016) and a Holocene transgression (van Engelen *et al* 2020) provided the boundary conditions, namely the change of the stage of, and border between, onshore and offshore surface water. These were conceptualized as assigned heads and concentrations of incoming water. Onshore surface water was conceptualized

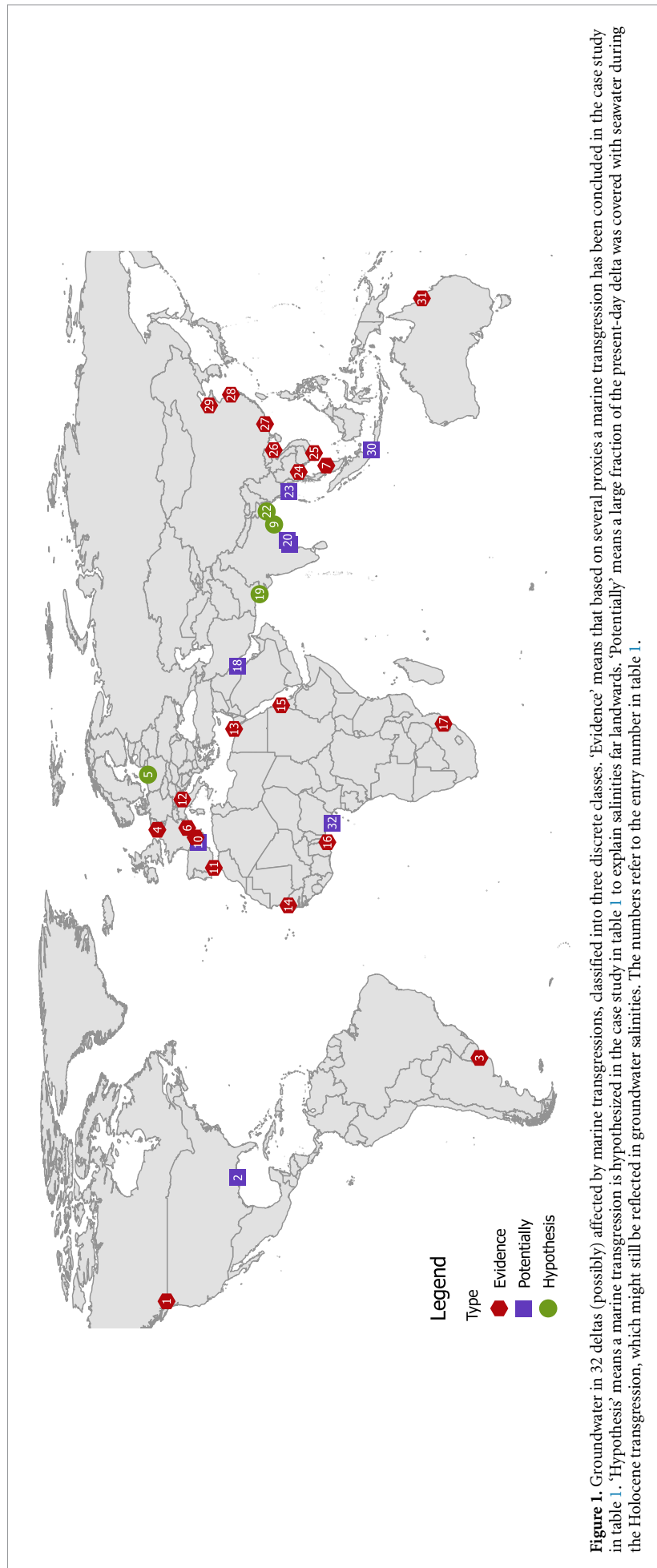


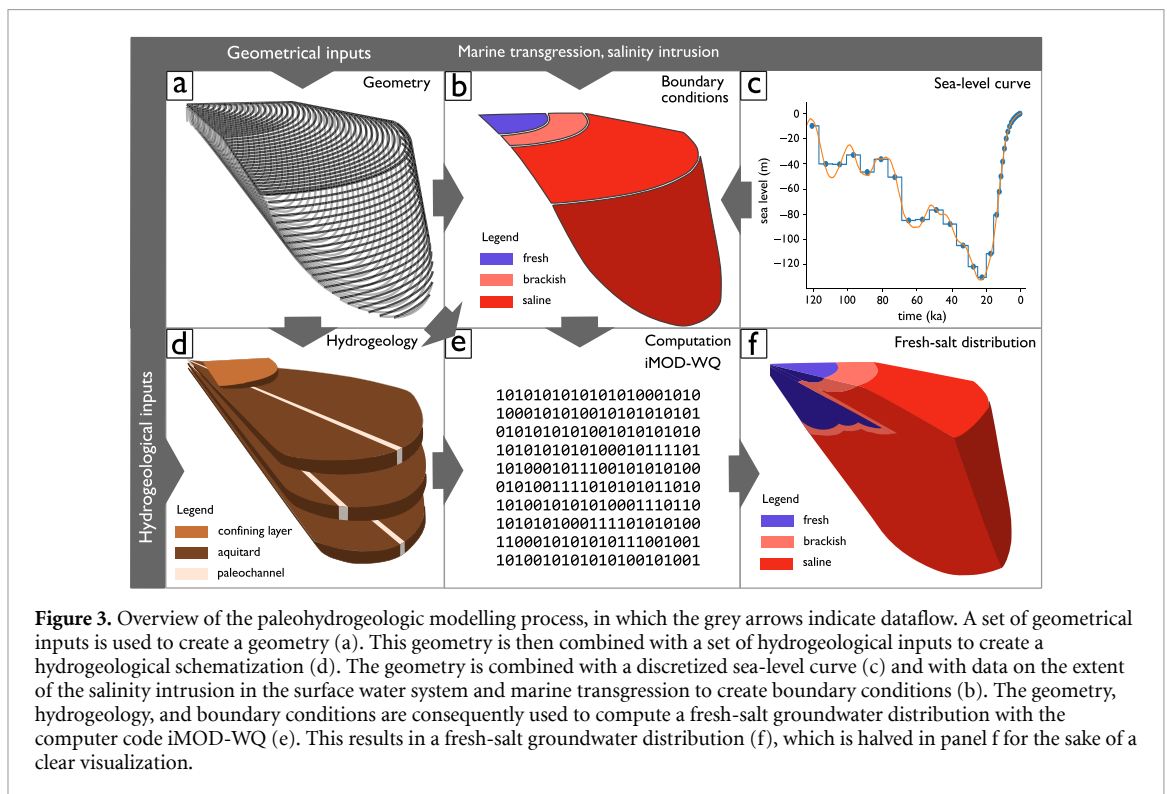
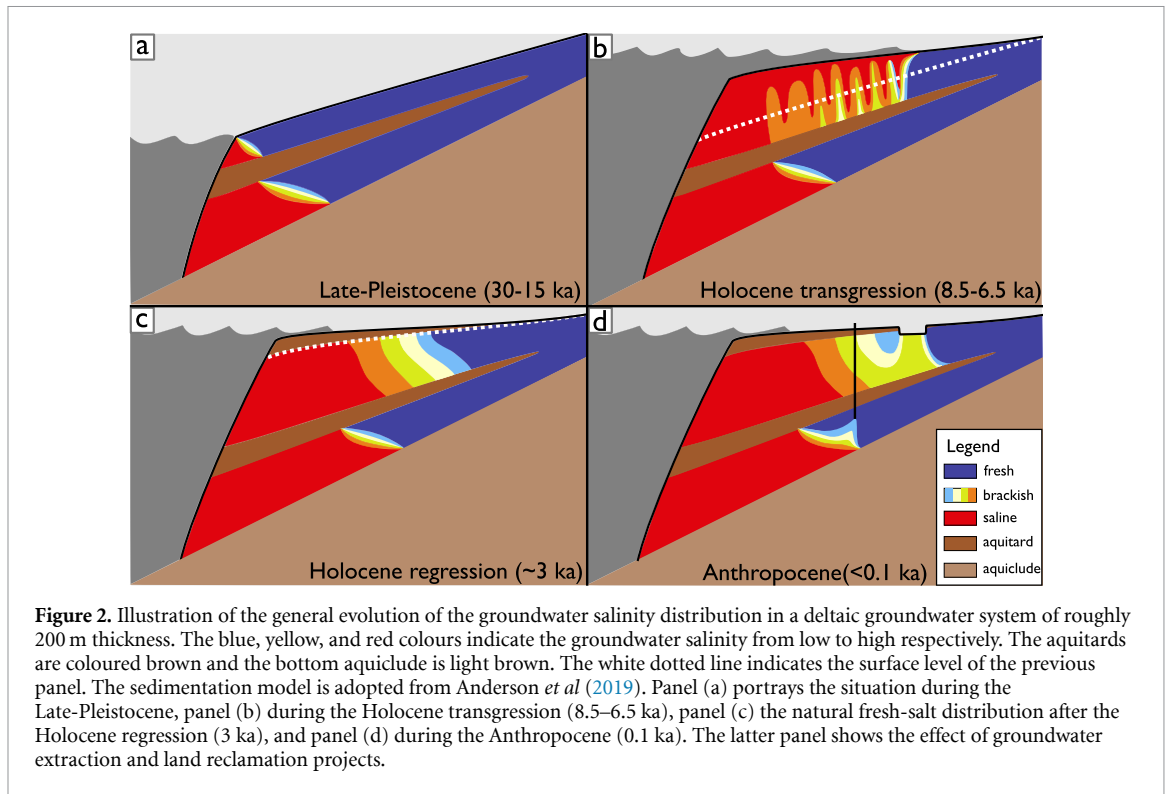
**Figure 1.** Groundwater in 32 deltas (possibly) affected by marine transgressions, classified into three discrete classes. ‘Evidence’ means that based on several proxies a marine transgression has been concluded in the case study in table 1. ‘Hypothesis’ means a marine transgression is hypothesized in the case study in table 1 to explain salinities far landwards. ‘Potentially’ means a large fraction of the present-day delta was covered with seawater during the Holocene transgression, which might still be reflected in groundwater salinities. The numbers refer to the entry number in table 1.

**Table 1.** Literature review of deltas with evidence for saline groundwater affected by marine transgressions. In the ‘Type’ column, ‘Evidence’ means that based on several proxies a marine transgression has been concluded in the case study; ‘Hypothesis’ means a marine transgression is hypothesized in the case study to explain salinities far landwards; ‘Potentially’ means a large fraction of the present-day delta was covered with seawater during the Holocene transgression, which might still be reflected in groundwater salinities. This table expands the initial table published in Larsen *et al* (2017).

No.	Delta	Country	Type	Proxies	Reference
1	Fraser	Canada	Evidence	Ions	Simpson and Hutcheon (1995)
2	Mississippi	United States	Potentially	Paleogeography	Törnqvist <i>et al</i> (2006), Stanton <i>et al</i> (2017)
3	Rio de la Plata	Argentina	Evidence	Ions	Santucci <i>et al</i> (2016)
4	Rhine-Meuse	Netherlands	Evidence	Ions, isotopes, groundwater ages, modelling, paleogeography	Delsman <i>et al</i> (2014)
5	Vistula	Poland	Hypothesis	Paleogeography	Kozerski (1983)
6	Rhone	France	Evidence	Ions, groundwater ages	de Montety <i>et al</i> (2008)
7	Kelantan	Malaysia	Evidence	Geophysics, ions	Samsudin <i>et al</i> (2008), Sefie <i>et al</i> (2018)
8	Llobregat	Spain	Evidence	Ions, isotopes	Manzano <i>et al</i> (2001)
9	Mahanadi	India	Hypothesis	Ions, (saline inversion)	Behera <i>et al</i> (2019)
10	Ebro	Spain	Potentially	Paleogeography	Edmunds (2001)
11	Doñana	Spain	Evidence	Ions, isotopes, noble gas	Manzano <i>et al</i> (2001)
12	Po	Italy	Evidence	Ions	Colombani <i>et al</i> (2017)
13	Nile	Egypt	Evidence	Ions, isotopes, paleogeography, modelling	Geirnaert and Laeven (1992), Geriessh <i>et al</i> (2015), van Engelen <i>et al</i> (2019)
14	Saloum	Senegal	Evidence	Ions (major and minor), isotopes, paleogeography	Ausseil-Badie <i>et al</i> (1991), Faye <i>et al</i> (2005)
15	Tokar	Sudan	Evidence	Ions	Elkrail and Obied (2013)
16	Volta	Ghana	Evidence	Isotopes, modelling	Akouvi <i>et al</i> (2008)
17	Incomati	Mozambique	Evidence	Ions, isotopes	Nogueira <i>et al</i> (2019)
18	Shatt al-Arab	Iraq	Potentially	Paleogeography	Cooke (1985)
19	Indus	Pakistan	Hypothesis	Ions	Naseem <i>et al</i> (2018)
20	Godovari	India	Potentially	Paleogeography	Prabaharan <i>et al</i> (2018)
21	Krishna	India	Potentially	Paleogeography	Prabaharan <i>et al</i> (2018)
22	Ganges-Brahmaputra	Bangladesh	Evidence	Ions, isotopes	Sarker <i>et al</i> (2018), Naus <i>et al</i> (2019)
23	Ayeyarwady	Myanmar	Potentially	Paleogeography	Giosan <i>et al</i> (2018)
24	Chao Phraya	Thailand	Hypothesis	Ions, isotopes	Yamanaka <i>et al</i> (2011), Stoecker <i>et al</i> (2013)
25	Mekong	Vietnam	Evidence	Geophysics, modelling, groundwater ages, ions	Bording <i>et al</i> (2017), Van Pham <i>et al</i> (2019), Tran <i>et al</i> (2020)
26	Red River	Vietnam	Evidence	Geophysics, modelling, isotopes	Tran <i>et al</i> (2012), Larsen <i>et al</i> (2017)
27	Pearl	China	Evidence	Ions, groundwater ages	Wang and Jiao (2012)
28	Yangtze	China	Evidence	Stratigraphy, ions	Chen <i>et al</i> (1997)
29	Yellow River	China	Evidence	Isotopes, ions, groundwater ages	Han <i>et al</i> (2011)
30	Ciliwung	Indonesia	Potentially	Paleogeography	Hehanussa (1980), Dirks <i>et al</i> (1989), Kooy <i>et al</i> (2016)
31	Burdekin	Australia	Evidence	Ions, isotopes, groundwater ages	Fass <i>et al</i> (2007)
32	Niger	Nigeria	Potentially	Paleogeography	Allen (1964), Anthony (1995)

as a linear decreasing profile of assigned heads from the delta apex to the coastline. The elevation and location of the apex were constant in height and location through time, whereas those of the coastline varied through time, driven by the sea level curve and

Holocene transgression. Salinity of the onshore surface water system was set with a linear salinity profile, emulating the effect of saline surface water intrusion. The models start initially completely saline, as it is assumed that the deltaic aquifers were completely



saline just after the marine transgression in the interglacial highstand 125 ka (Zamrsky *et al* 2020). This initially saline groundwater is traced with a separate tracer in the solute transport component of the model, to get a sense of the memory of the groundwater system (Post *et al* 2013, Delsman *et al* 2014). For further details, the reader is guided to the extended model description in appendix A. The simulations

were computed with the iMOD-WQ code (Verkaik *et al* 2021), which allows for parallelization, on the Dutch national supercomputer (Surfsara 2014).

### 3.2. Metrics

Our simulations computed equivalent present-day fresh-salt groundwater distributions for 15 deltas under natural conditions, named ‘end-state’ in the

rest of this paper. ‘End-state’ therefore refers to the results of the final timestep of the results, which represent the natural groundwater salinity distribution. In other words, the effects of groundwater extractions were not included in the model simulations. These effects, however, were corrected for in the analysis of the results, as described further. To characterize the volumes of fresh groundwater and compare between deltas we used the following metrics. Firstly,  $V_{fw,on}$  and  $V_{fw,off}$  which are respectively the total onshore and offshore volumes of natural fresh groundwater up to 300 m depth. Groundwater is only rarely extracted beyond this 300 m limit (Perrone and Jasechko 2017), as this is generally economically unfeasible (Wittmeyer *et al* 1996). Secondly,  $S_{init}$  is the mass fraction of initial salt (initial condition of the paleo-hydrogeologic model 125 ka ago) still present in the entire model domain over the total salt mass. Finally,  $t_d$  is the exhaustion time, which is the time until the onshore fresh groundwater is exhausted, when taking only the diffuse recharge of infiltrated rainfall into account. This was calculated as:

$$t_d = \frac{V_{fw,on} - \int_{1958}^{2013} (Q - R) dt}{Q_{t=2014} - R_{t=2014}} \quad (1)$$

where  $Q$  is the total yearly groundwater extraction flux of the delta and  $R$  is the yearly diffuse groundwater recharge of infiltrated rainfall in the delta. Values for  $Q$  were obtained from simulations of the years 1958 up to 2014 of the global hydrological model ‘PCRaster Global Water Balance’ (PCR-GLOBWB), which computed daily groundwater extraction rates based on water demand and surface water availability (Sutanudjaja *et al* 2018). This time frame covers the period when groundwater overpumping started in most of the deltas (Burdekin: Narayan *et al* 2007, Chao Phraya: Yamanaka *et al* 2011, Ganges-Brahmaputra: Michael and Voss 2009a, Mekong: Minderhoud *et al* 2017, Nile: Switzman *et al* 2015, Po: Teatini *et al* 2006, Saloum: Dieng *et al* 2017, Yangtze: Xue *et al* 2008, Yellow River: Cao *et al* 2016), except in two cases (Rhine-Meuse and Red River) where localized overpumping occurred already around 1900 (Rhine-Meuse: Delsman *et al* 2014, Red River: Winkel *et al* 2011). When  $R$  exceeded  $Q$ ,  $Q - R$  is set to 0, as we assumed that any excess recharge water is drained by the surface water system. The rationale behind  $t_d$  is that it relates to the theoretical volume of ‘clean’ fresh groundwater that can be pumped. After this time, this volume is exhausted and a) partly taken out of storage, leading to head decline; b) mostly replaced by (often brackish or polluted) river water from concentrated recharge or by sea water. The definition of  $t_d$  does therefore not account for enhanced recharge from rivers (Bredehoeft 2002). Moreover,  $t_d$  does not include local-scale problems due to overpumping, such as saline groundwater upconing. Instead, the underlying assumption is that

whenever a groundwater well salinizes, a new one is immediately created to pump in a region with fresh groundwater. To restrict understating the problem of groundwater salinization, we considered deltas with a logarithmic mean  $t_d$  of less than 200 years at high risk. Deltas that cross the 200-year threshold only after increasing  $Q$  4 times, equaling the predicted increase in groundwater extraction for the Nile Delta (Mabrouk *et al* 2018), were appointed a medium risk.

### 3.3. Validation

Validating our fresh groundwater volume estimates is challenging as data is limited. To utilize the available data as much as possible, three approaches were taken. Firstly, we compared our simulated volumes to three-dimensional distributions inferred from observations (Rhine-Meuse: Delsman *et al* 2020; Mekong: Gunnink *et al* 2021) or computed by a detailed regional model (Nile: van Engelen *et al* 2019). Secondly for some deltas, a volume was estimated based on reported cross-sections and maps of the groundwater salinity distribution (Ganges-Brahmaputra: Sarker *et al* 2018; Red River: Larsen *et al* 2017; Kelantan: Samsudin *et al* 2008, Saloum: Faye *et al* 2005). In this case the reported maps were georeferenced (QGIS Development Team 2021), and multiplied with reported aquifer thicknesses to compute volumes. Thirdly, as a form of indirect validation we used reported depth distributions of local well data to infer if our fresh-salt distribution approached reality sufficiently with the following simple decision scheme. For each  $x, y$  location in the model, wells are dug until an aquifer is found that contains no salt in the vertical direction, up to a limit of 300 m. That is, if the upper aquifer is saline, the well filter will be placed in the first aquifer that is fresh below it, where we have used 20 m under its confining layer, as suggested in Wittmeyer *et al* (1996). In this way well distributions are created with depth that can be compared to the local data (Nile: van Engelen *et al* 2019, Rhine-Meuse: De Lange *et al* 2014, Mekong: Minderhoud *et al* 2017). Total extraction rates were also compared between the three regional datasets and PCR-GLOBWB simulations. The total extraction rates estimated in Michael and Voss (2009a) for the Ganges-Brahmaputra were added to this comparison.

## 4. Results

### 4.1. Groundwater well depths as indirect validation

Figure 4 shows a comparison between the observed and simulated depth distributions of groundwater wells. In general, most simulations were not able to capture the well depth distributions. In the Nile Delta, groundwater is mainly extracted at 50 m depth, whereas our simulated distributions seem to avoid this depth. We attribute these differences to our simplification of the confining layer. In reality, the thickness of this layer increases from a few meters

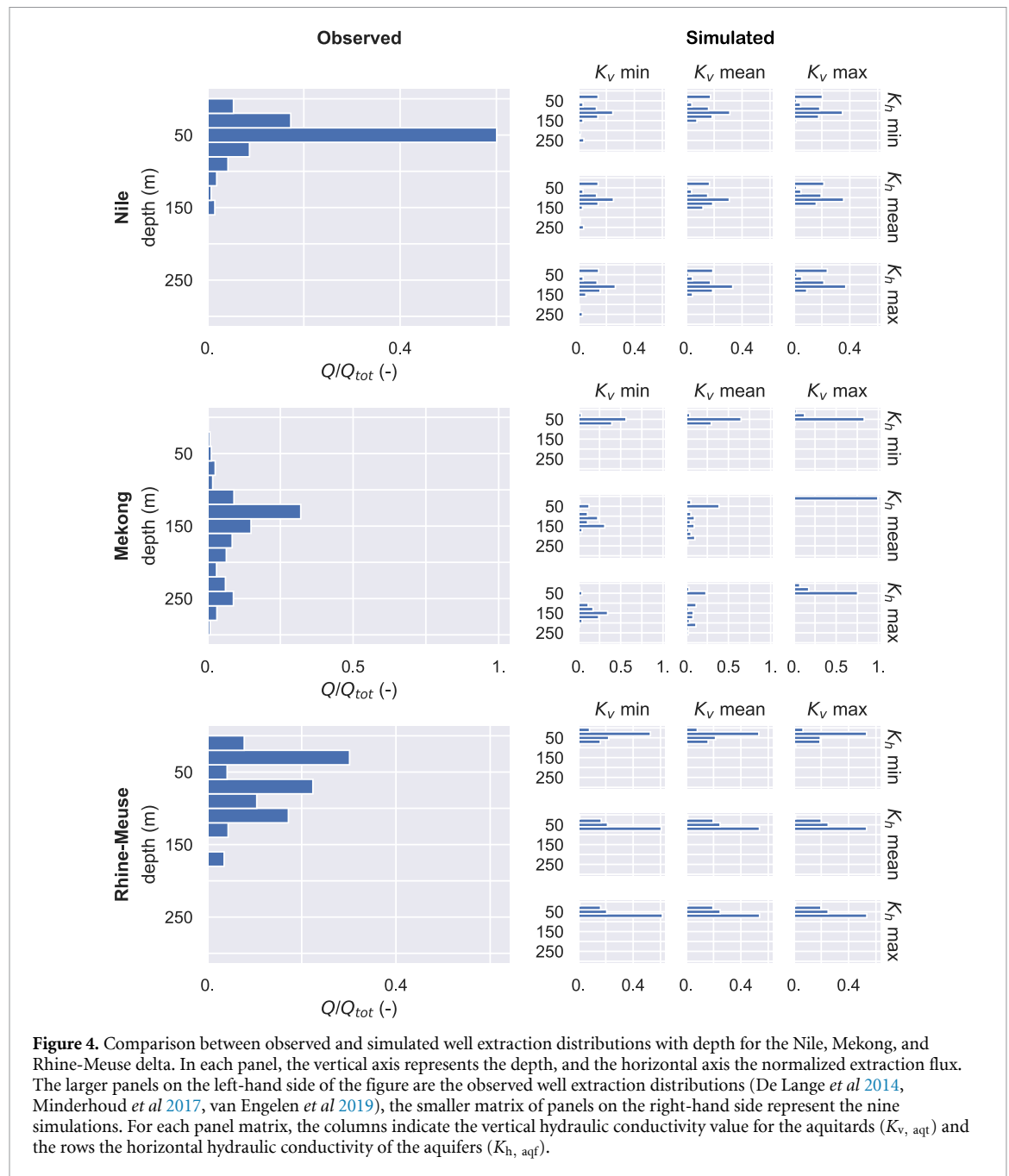


**Table 2.** A comparison between total groundwater extraction rates in regional datasets and simulated by PCR-GLOBWB. The ‘factor’ column states the division between these two datasets.

Delta	Regional dataset ( $10^6 \text{ m}^3 \text{ d}^{-1}$ )	PCR-GLOBWB ( $10^6 \text{ m}^3 \text{ d}^{-1}$ )	Factor (—)
Mekong	2.4	2.2	1.1
Nile	7.2	1.8	4.0
Rhine-Meuse	3.2	7.7	0.41
Ganges-Brahmaputra	150	35	4.3

at the apex to nearly 100 m near the coast with strong lateral variation (Pennington *et al* 2017). In our model, the thickness increased linearly from apex

to coast, without any variation. Furthermore, the poor quality of the surface water (Rasmussen *et al* 2009) is a reason to deepen wells, which was unaccounted for in our approach. For the Mekong delta, there are two simulations that replicated the observed well depth distributions, namely the simulations that have low conductive aquitards and high conductive aquifers allowing the existence of a salinity inversion (van Engelen *et al* 2020). The other simulations all simulate fresh groundwater in the upper aquifer, which is not observed in the field (Van Pham *et al* 2019). For the Rhine-Meuse delta, the models with a low aquifer hydraulic conductivity seemed to reproduce the observed well depth distribution the best. These simulations captured the low number of wells at 10 m depth and the peak in wells at 30 m depth.

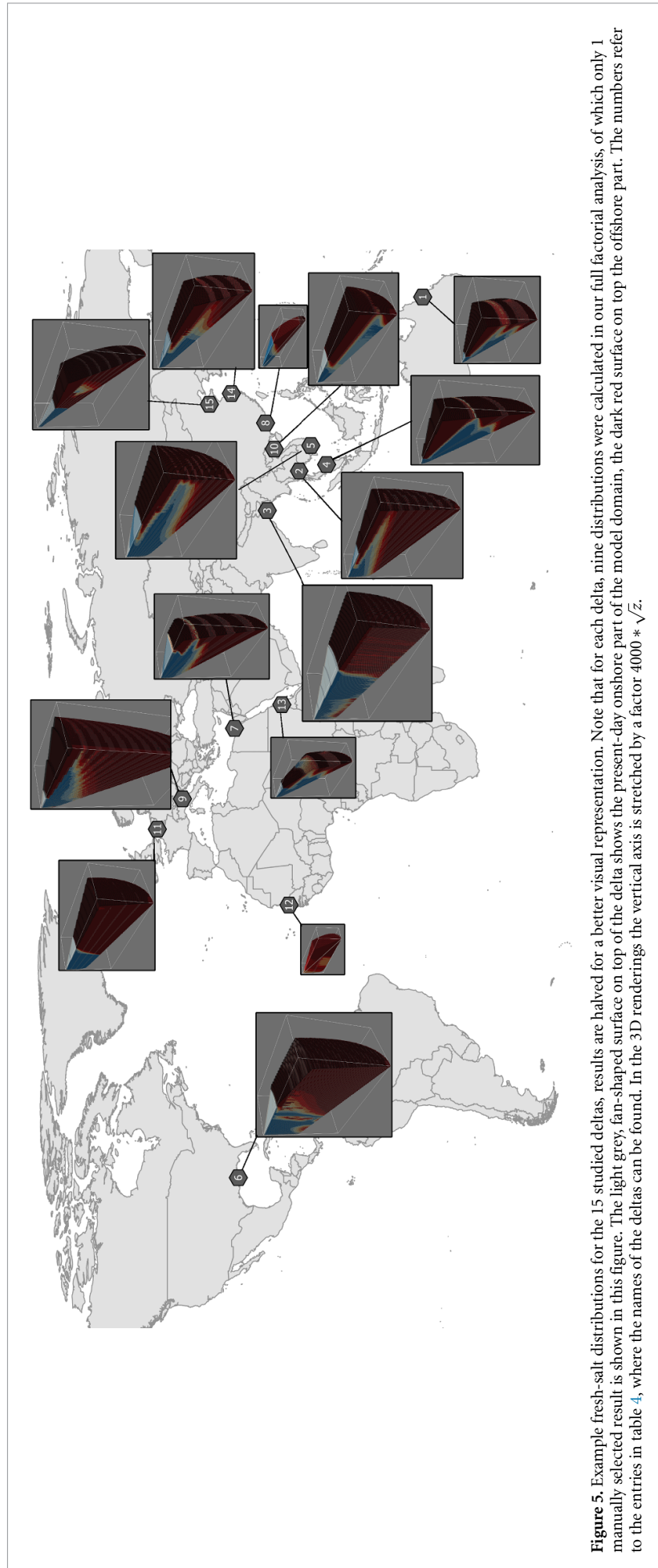


**Figure 5.** Example fresh-salt distributions for the 15 studied deltas, results are halved for a better visual representation. Note that for each delta, nine distributions were calculated in our full factorial analysis, of which only 1 manually selected result is shown in this figure. The light grey, fan-shaped surface on top of the delta shows the present-day surface of the model domain, the dark red surface on top the offshore part. The numbers refer to the entries in table 4, where the names of the deltas can be found. In the 3D renderings the vertical axis is stretched by a factor  $4000 * \sqrt{z}$ .

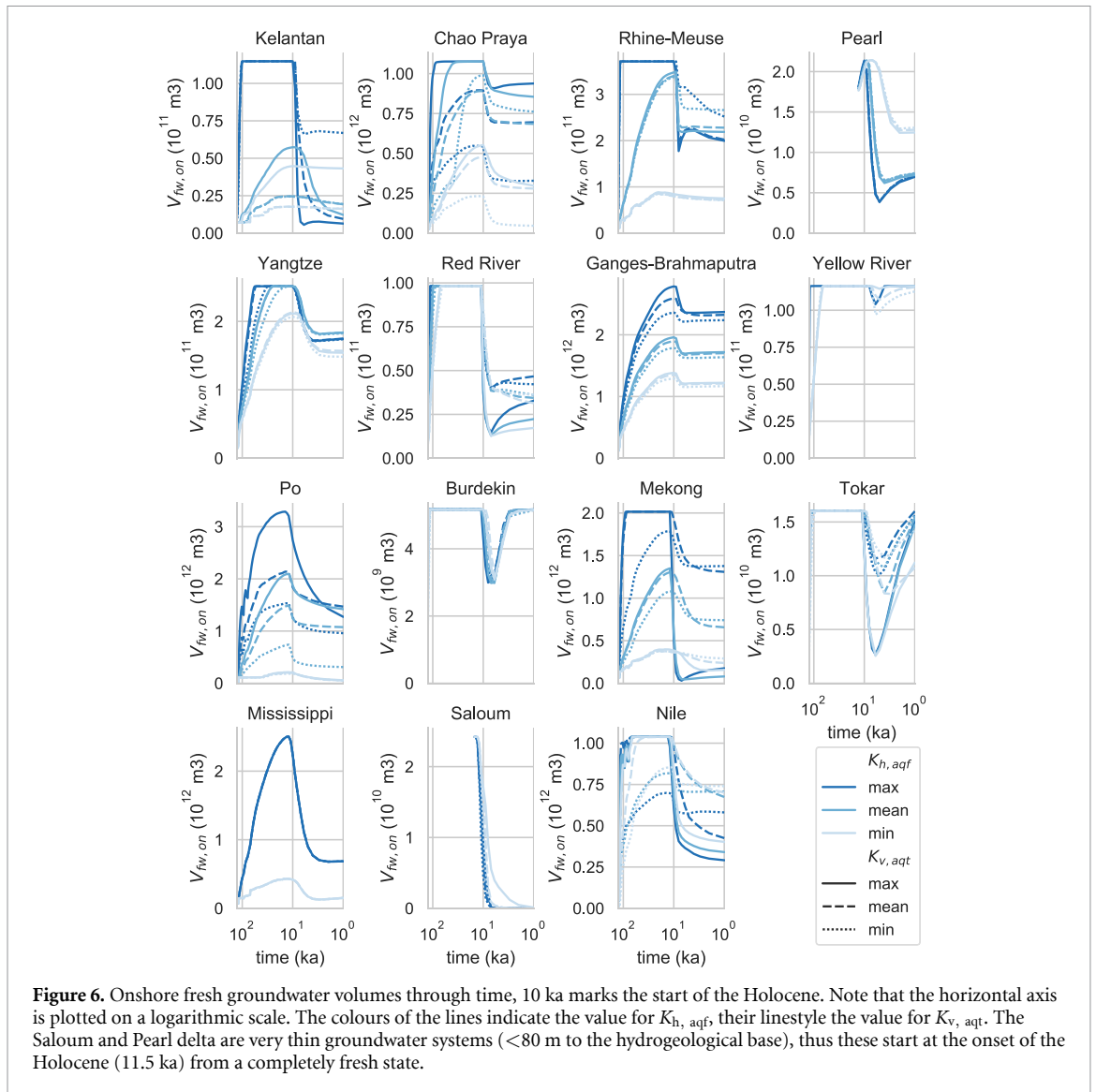


**Figure 6.** Onshore fresh groundwater volumes through time, 10 ka marks the start of the Holocene. Note that the horizontal axis is plotted on a logarithmic scale. The colours of the lines indicate the value for  $K_{h,aqf}$ , their linestyle the value for  $K_{v,aqt}$ . The Saloum and Pearl delta are very thin groundwater systems (<80 m to the hydrogeological base), thus these start at the onset of the Holocene (11.5 ka) from a completely fresh state.

The tail of the depth distribution was not simulated, presumably due to the simplifications in our lithological model. We also checked the total extracted fluxes in the available extraction data to the simulated PCR-GLOBWB data, shown in table 2. This table shows that considerable differences can exist. The total extraction rates in the Mekong delta were simulated quite well by PCR-GLOBWB but were underestimated in the Nile and the Ganges-Brahmaputra delta and overestimated in the Rhine-Meuse delta.

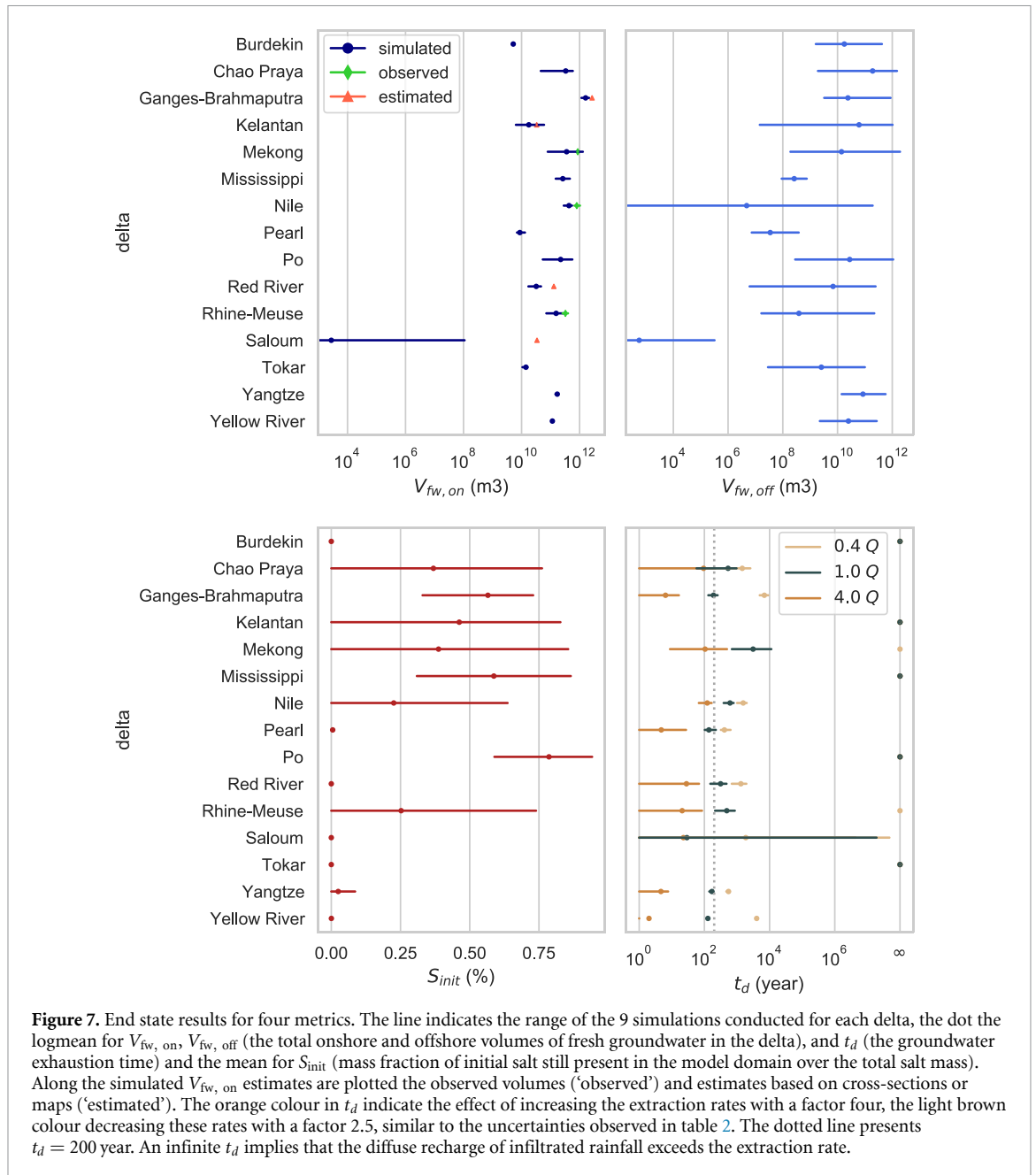
#### 4.2. End-state fresh-salt distributions

Figure 5 shows example end-state fresh-salt distributions for 15 deltas. The wide variability in geometry is visible. For example, the groundwater system of the Pearl delta (No. 8 in figure 5) is significantly shallower than the thick Po delta (No. 9 in figure 5). It also shows that in some simulations, for example the Kelantan (No. 4), a vast amount of fresh groundwater is located offshore underneath clay layers, indicating the system is not in equilibrium (Kooi *et al* 2000, Zamrsky *et al*

2022). Several phases sketched in figure 2 are visible in the shown end-state distributions. For example, in the Mississippi (No. 6), saline fingers formed by free convection are still visible (figure 2(b)). This delta has a lot of clay layers and paleochannels, following the conceptual model of (Griffith 2003), causing fingers of salt water to persist in the deep groundwater system after the Holocene transgression. The Kelantan delta (No. 4) clearly shows a saline upper aquifer and fresh lower aquifers just like in figure 2(c). In the Po delta (No. 9) a cone develops towards the onshore, following figure 2(d).

#### 4.3. Fresh groundwater volumes through time

Figure 6 presents the time series of the total volume of fresh groundwater onshore ( $V_{fw,on}$ ) over 125 ka. Fresh groundwater volumes increase throughout the Pleistocene, after which they rapidly decline during the marine transgression that marks the start of the Holocene (note the logarithmic horizontal axis). In some small deltas, namely the Burdekin and the



**Figure 7.** End state results for four metrics. The line indicates the range of the 9 simulations conducted for each delta, the dot the logmean for  $V_{fw, on}$ ,  $V_{fw, off}$  (the total onshore and offshore volumes of fresh groundwater in the delta), and  $t_d$  (the groundwater exhaustion time) and the mean for  $S_{init}$  (mass fraction of initial salt still present in the model domain over the total salt mass). Along the simulated  $V_{fw, on}$  estimates are plotted the observed volumes ('observed') and estimates based on cross-sections or maps ('estimated'). The orange colour in  $t_d$  indicate the effect of increasing the extraction rates with a factor four, the light brown colour decreasing these rates with a factor 2.5, similar to the uncertainties observed in table 2. The dotted line presents  $t_d = 200$  year. An infinite  $t_d$  implies that the diffuse recharge of infiltrated rainfall exceeds the extraction rate.

Tokar, a full recovery from this transgression to the Pleistocene fresh groundwater volume is simulated as the delta prograded, but in most cases  $V_{fw, on}$  does not recover. In the very thick groundwater systems (Ganges-Brahmaputra, Po, Nile, and Mekong), it seems that  $V_{fw}$  has not reached its potential maximum value in one glacial cycle. Thus, for these systems  $V_{fw}$  is a conservative estimate, because of our salt initial condition. Given more glacial cycles, which have relative long periods of low sea level,  $V_{fw}$  would likely be larger in these large deltas. In most cases, the range in estimated  $V_{fw}$  values is mainly caused by the uncertainty in the horizontal hydraulic conductivity of the aquifers, with the Nile delta as exception where the properties of the aquitards are much more uncertain (van Engelen *et al* 2019).

**4.4. End-state metrics and further validation**

Figure 7 presents the end-state metrics for the 15 deltas (see table 4 for the results in a table). Most deltas have an onshore fresh groundwater volume ( $V_{fw, on}$ ) ranging from  $10^{10}$  to  $10^{12}$  m<sup>3</sup>, with the main exception being the Saloum delta in Senegal which has a very shallow groundwater system and a saline surface water system. In all cases where there are observations to validate  $V_{fw, on}$  estimates based on simulations, The Mekong delta, the Rhine-Meuse delta and Nile delta, our the logmeans of the simulations are on the conservative side. The estimates based on reported maps and cross-sections (Ganges-Brahmaputra, Red River, Kelantan, and Saloum) are in agreement with this. The hydrogeology of Saloum delta is presumably not well captured

in our model, as the simulated  $V_{fw, on}$  has a high variance and differs a lot from the estimated  $V_{fw, on}$  based on cross-sections. The variance in  $V_{fw, on}$  estimates is small compared to the variance in the offshore fresh groundwater volumes ( $V_{fw, off}$ ), which is controlled more by free-convection. Furthermore, the logarithmic means of these offshore volumes are usually at least an order of magnitude smaller than their onshore counterparts, except for the Burdekin and Kelantan delta. This is because the offshore domain of these two deltas is a lot larger than its onshore counterpart. It can also be seen that the residence times of salt in many deltas presumably exceeds that of a glaciation cycle, as  $S_{init}$  often has a value higher than 0%. Finally, we observe that four of the simulated deltas have an expected exhaustion time ( $t_d$ ) that is shorter than 200 years. The deltas with low extraction rates in the PCR-GLOBWB data (Tokar) or a high recharge (Mississippi, Po, Kelantan, Burdekin) have a large exhaustion time. Multiplying extractions by a factor four causes nine of the deltas to have a  $t_d$  shorter than 200 years. The exhaustion time  $t_d$  of the Saloum delta varies strongly because of its low extraction rate and strongly varying  $V_{fw, on}$ .

## 5. Discussion and conclusion

We have conducted paleohydrogeologic reconstructions for 15 deltas across the world, varying widely in geometry, lithology, and boundary conditions. The results show that fresh groundwater resources of these areas have experienced large changes over time, especially at the start of the Holocene (9 ka), when the eustatic sea level increased rapidly. The fresh groundwater resources of two simulated smaller deltas, namely the Burdekin and Tokar, experience a complete recovery to Pleistocene freshwater volumes after the Holocene transgression. In the field, traces of the past marine transgressions are still found in these deltas (Fass *et al* 2007, Elkrail and Obied 2013), thus the fresh groundwater volumes in these small deltas are presumably overestimated. A possible explanation for this overestimation is that a single porosity model, as used in this research, is not able to capture the tailing of a passing salt front. A dual-porosity model manages to capture this phenomenon (Lu *et al* 2009), which would result in a slower flushing of salt water after the Holocene transgression. For the larger deltas, however, our simulations possibly underestimate the available onshore fresh groundwater resources ( $V_{fw, on}$ ), as shown by The Red River, the Nile, Rhine-Meuse, and to a lesser degree the Mekong, Ganges-Brahmaputra and Kelantan delta in figure 7. Nearly all deltas possess onshore fresh groundwater volumes that range between  $10^{10}$  to  $10^{12}$  m<sup>3</sup> (2 [Red River] to 280 [Po] m<sup>3</sup>/m<sup>2</sup>) and offshore fresh groundwater volumes that are presumably one or more orders of magnitude smaller. Comparing these volumes to present-day recharge of infiltrated

rainfall and extraction rates shows that four deltas have a fresh groundwater exhaustion time  $t_d$  of less than 200 years and are presumably at risk, another four might be at risk with increasing extractions, and six deltas have a low risk since they receive ample recharge of infiltrated rainfall or have little groundwater extractions. The  $t_d$  computed for the Saloum delta had a very high variance.

Table 3 provides, based on literature, the reasons why groundwater is used rather than surface water in the considered deltas. We observe that groundwater is extracted for water quality reasons in most deltas, the Burdekin being the only exception. The most common issues with surface water are salinity, caused by either tidal differences or evapoconcentration, and nutrients, often caused by over fertilization or human waste effluents. Ten deltas experience saline surface water, and eight deltas experience an abundance of nutrients in their surface water. In only five deltas, groundwater was extracted for quantitative reasons because of surface water scarcity. We have listed whether deltas have saline surface water and their exhaustion risk ( $t_d < 200$  years) in table 4. Note that the Nile and Rhine-Meuse were appointed respectively a high and low risk, instead of a medium risk, as we corrected their extraction rates with the available field data, and thus respectively used 4.0 Q and 0.4 Q for these deltas (table 2). Furthermore, the Saloum was appointed an uncertain risk given the high variance in  $V_{fw, on}$ . There are four deltas that have both a high fresh groundwater exhaustion risk and surface water salinity issues, namely the Ganges-Brahmaputra, the Nile, the Pearl, the Yangtze delta. The Mekong and Red River delta, also suffering from saline surface water, currently possess ample fresh groundwater resources, but are seriously under pressure with increasing extractions.

The definition of  $t_d$  does not account for enhanced recharge from rivers (Bredehoeft 2002), which is likely the main source of groundwater recharge in case of intensive pumping in deltaic areas. We deliberately left this term out of the sustainability measure  $t_d$ , because the usefulness of riverine recharge for freshwater supply is questionable. Groundwater is usually extracted in deltas because of an insufficient surface water quality (table 3). Riverine recharge contaminated with pollutants that break down or are adsorbed to sediments might be good enough for extraction after treatment. An example of this is the Rhine water that is first treated and then used to artificially recharge drinking water resources in the Netherlands (Stuyfzand 1997). However, when surface water is saline, riverine recharge will progressively salinize groundwater resources, gradually rendering these resources unusable. This is the case for 10 out of the studied 15 deltas (tables 3 and 4), so for these at least  $t_d$  is a useful metric. A combination of a low  $t_d$  and saline recharge leads to progressively saline groundwater resources on a human timescale,

**Table 3.** Reasons for groundwater extraction for 15 deltas. The ID column refers to the symbol number in figures 5 and B1.

Delta	ID	Reasons to extract groundwater		References
		Problems with water quantity	Problems with water quality surface water	
Burdekin	1	Surface water scarcity (dry season)	—	Davis <i>et al</i> (2014)
Chao Praya	2	—	Bacteria, Nutrients, Turbidity	Simachaya <i>et al</i> (2000)
Ganges-Brahmaputra	3	Surface water scarcity (dry season)	Salinity, Nutrients	Shamsudduha <i>et al</i> (2011), Ayers <i>et al</i> (2016)
Kelantan	4	—	Turbidity (sediments)	Sefie <i>et al</i> (2018)
Mekong	5	—	Salinity, Nutrients	Minderhoud <i>et al</i> (2017), Eslami <i>et al</i> (2021)
Mississippi	6	—	Salinity, Temperature (Energy plants)	LGWRC (2012), LPHI and AAE (2016)
Nile	7	—	Salinity, Nutrients	El-Agha <i>et al</i> (2017)
Pearl	8	—	Salinity, Nutrients	Lu <i>et al</i> (2009), Shi and Jiao (2014)
Po	9	—	Salinity	Giambastiani <i>et al</i> (2013), Colombani <i>et al</i> (2016)
Red River	10	—	Salinity, Nutrients,	Ca <i>et al</i> (1994), Hoang <i>et al</i> (2018)
Rhine-Meuse	11	Surface water scarcity	Nutrients, Pesticides	Pellenbarg (1997), Oude Essink <i>et al</i> (2010)
Saloum	12	—	Salinity	Faye <i>et al</i> (2005)
Tokar	13	Surface water scarcity	Salinity	Elkrail and Obied (2013)
Yangtze	14	—	Salinity, Nutrients,	Dai <i>et al</i> (2011), Shi <i>et al</i> (2012)
Yellow River	15	—	Nutrients	Chen <i>et al</i> (2007), Fan <i>et al</i> (2012)

which means the delta's capacity to withstand periods of water scarcity decreases. This combination exists in four deltas (Ganges-Brahmaputra, Nile, Pearl, and Yangtze), and arises in two more deltas with increased extraction rates (Mekong and Red River) (table 4).

Some further remarks should be made on  $t_d$ . A  $t_d$  of 200 years does not mean that the fresh groundwater volumes are safeguarded for 200 years. Before  $t_d$  is reached, deltas already face more local-scale problems from groundwater extraction, such as enhanced salt water intrusion (Michael *et al* 2017) and upconing (Werner *et al* 2013, Pauw *et al* 2015). In the latter case, pumping results in a rise of saline groundwater (Jakovovic *et al* 2016) and furthermore the induced vertical groundwater velocities will increase mechanical dispersion and cause mixing of fresh and saline groundwater (Zhou *et al* 2005). The latter process increases the salinity of the pumped groundwater becoming saline, making it unusable. Underneath abandoned wells, a thick brackish zone can persist for tens of years, significantly hindering the restart of these wells (Zhou *et al* 2005). An example of these local-scale problems can be found in the

Rhine-Meuse delta, where issues with saline groundwater do exist near the coast despite it having a low risk in table 4 (Delsman *et al* 2018).

Another remark is that  $t_d$  will presumably decrease, since extraction rates are expected to increase in most areas, as can be seen for a fourfold increase in extraction rates in figure 7. Reducing extractions, on the other hand, can increase  $t_d$  by an order of magnitude. The fourfold increase of  $Q$  in figure 7 may seem large, but mind that similar increases are expected for deltas with a booming population, such as the Nile Delta (Mabrouk *et al* 2018). In addition, PCR-GLOBWB underestimated total extraction rates in the Nile Delta and Ganges-Brahmaputra from local data by a factor four. PCR-GLOBWB's water allocation scheme has a tendency to underestimate extraction rates in deltas, as the current version of the model does not incorporate the effects of surface water quality (Sutanudjaja *et al* 2018). Since in terms of water quantity, ample surface water is usually available in most deltas, groundwater is only extracted mainly because of an insufficient surface water quality (table 3). On the other hand,

**Table 4.** End state results.  $V_{fw}$  here stands for the onshore fresh water volume ( $m^3$ ), the min, avg, max, obs, est suffixes respectively stand for minimum, logmean, maximum, observed, and estimated.  $Q$  and  $R$  is the extracted groundwater and recharge flux ( $m^3/d$ ).  $t_d$  is the exhaustion time ( $y$ ), the  $q5$  suffix indicates the exhaustion time computed using a  $Q$  multiplied with a factor 4 and 'Risk' is the risk of groundwater exhaustion.

Delta	$V_{fw, min}$	$V_{fw, avg}$	$V_{fw, max}$	$V_{fw, obs}$	$V_{fw, est}$	$Q$	$R$
Burdekin	$5.1 \times 10^{+09}$	$5.2 \times 10^{+09}$	$5.2 \times 10^{+09}$			$1.8 \times 10^{+05}$	$5.8 \times 10^{+06}$
Chao Praya	$4.6 \times 10^{+10}$	$3.3 \times 10^{+11}$	$5.8 \times 10^{+11}$			$6.2 \times 10^{+08}$	$2.8 \times 10^{+07}$
Ganges-Brahmaputra	$1.2 \times 10^{+12}$	$1.6 \times 10^{+12}$	$2.1 \times 10^{+12}$			$2.7 \times 10^{+12}$	$5.0 \times 10^{+09}$
Kelantan	$6.4 \times 10^{+09}$	$1.8 \times 10^{+10}$	$5.9 \times 10^{+10}$			$3.3 \times 10^{+10}$	$2.7 \times 10^{+07}$
Mekong	$8.0 \times 10^{+10}$	$3.6 \times 10^{+11}$	$1.3 \times 10^{+12}$	$8.7 \times 10^{+11}$		$8.0 \times 10^{+08}$	$6.8 \times 10^{+08}$
Mississippi	$1.5 \times 10^{+11}$	$2.6 \times 10^{+11}$	$4.6 \times 10^{+11}$			$3.5 \times 10^{+07}$	$1.2 \times 10^{+09}$
Nile	$2.9 \times 10^{+11}$	$4.3 \times 10^{+11}$	$5.5 \times 10^{+11}$	$8.1 \times 10^{+11}$		$6.6 \times 10^{+08}$	$0.0 \times 10^{+00}$
Pearl	$7.0 \times 10^{+09}$	$8.7 \times 10^{+09}$	$1.3 \times 10^{+10}$			$5.2 \times 10^{+07}$	$1.8 \times 10^{+06}$
Po	$5.4 \times 10^{+10}$	$2.2 \times 10^{+11}$	$5.6 \times 10^{+11}$			$8.6 \times 10^{+02}$	$2.9 \times 10^{+08}$
Red River	$1.7 \times 10^{+10}$	$3.2 \times 10^{+10}$	$4.7 \times 10^{+10}$			$1.1 \times 10^{+08}$	$2.3 \times 10^{+07}$
Rhine-Meuse	$7.2 \times 10^{+10}$	$1.6 \times 10^{+11}$	$2.7 \times 10^{+11}$	$3.3 \times 10^{+11}$		$6.4 \times 10^{+08}$	$3.4 \times 10^{+08}$
Saloum	$0.0 \times 10^{+00}$	$2.8 \times 10^{+03}$	$1.1 \times 10^{+08}$			$3.4 \times 10^{+10}$	$0.0 \times 10^{+00}$
Tokar	$1.1 \times 10^{+10}$	$1.4 \times 10^{+10}$	$1.6 \times 10^{+10}$			$1.8 \times 10^{+04}$	$6.9 \times 10^{+06}$
Yangtze	$1.5 \times 10^{+11}$	$1.7 \times 10^{+11}$	$1.8 \times 10^{+11}$			$8.5 \times 10^{+08}$	$6.2 \times 10^{+07}$
Yellow River	$1.1 \times 10^{+11}$	$1.2 \times 10^{+11}$	$1.2 \times 10^{+11}$			$1.2 \times 10^{+09}$	$4.6 \times 10^{+08}$

Delta	$t_d min$	$t_d avg$	$t_d max$	$t_d avg, q5$	Risk	Saline surface water
Burdekin	$\infty$	$\infty$	$\infty$	$\infty$	Low	Not Present
Chao Praya	$5.8 \times 10^{+01}$	$5.3 \times 10^{+02}$	$9.6 \times 10^{+02}$	$9.4 \times 10^{+01}$	Medium	Not Present
Ganges-Brahmaputra	$1.3 \times 10^{+02}$	$1.9 \times 10^{+02}$	$2.5 \times 10^{+02}$	$6.4 \times 10^{+00}$	High	Present
Kelantan	$\infty$	$\infty$	$\infty$	$\infty$	Low	Not Present
Mekong	$7.0 \times 10^{+02}$	$3.1 \times 10^{+03}$	$1.1 \times 10^{+04}$	$1.1 \times 10^{+02}$	Medium	Present
Mississippi	$\infty$	$\infty$	$\infty$	$\infty$	Low	Present
Nile	$3.9 \times 10^{+02}$	$6.1 \times 10^{+02}$	$7.9 \times 10^{+02}$	$1.2 \times 10^{+02}$	High <sup>a</sup>	Present
Pearl	$1.0 \times 10^{+02}$	$1.4 \times 10^{+02}$	$2.2 \times 10^{+02}$	$4.8 \times 10^{+00}$	High	Present
Po	$\infty$	$\infty$	$\infty$	$\infty$	Low	Present
Red River	$1.5 \times 10^{+02}$	$3.1 \times 10^{+02}$	$4.8 \times 10^{+02}$	$2.8 \times 10^{+01}$	Medium	Present
Rhine-Meuse	$2.1 \times 10^{+02}$	$4.9 \times 10^{+02}$	$8.5 \times 10^{+02}$	$2.1 \times 10^{+01}$	Low <sup>a</sup>	Not Present
Saloum	$1.0 \times 10^{+00}$	$2.9 \times 10^{+01}$	$1.9 \times 10^{+07}$	$2.3 \times 10^{+01}$	Uncertain	Present
Tokar	$\infty$	$\infty$	$\infty$	$\infty$	Low	Present
Yangtze	$1.4 \times 10^{+02}$	$1.7 \times 10^{+02}$	$1.9 \times 10^{+02}$	$4.6 \times 10^{+00}$	High	Present
Yellow River	$1.2 \times 10^{+02}$	$1.3 \times 10^{+02}$	$1.3 \times 10^{+02}$	$2.0 \times 10^{+00}$	High	Not Present

<sup>a</sup> The risk of the Nile and Rhine-Meuse delta have been respectively increased and decreased, because local data for  $Q$  was available.

the higher extraction rates of PCR-GLOBWB in the Rhine-Meuse delta are presumably caused by the fact that our model area does not include the ice-pushed sandy moraines. Many extractions in the Netherlands are located in these moraines, because of its good water quality (Stuyfzand and Stuurman 2006, De Lange *et al* 2014).

The uncertainty propagated by  $Q$  affected  $t_d$  more severely than the uncertainty propagated by  $V_{fw, on}$ . The Rhine-Meuse and Nile delta both showed strong error in extracted groundwater (table 2), which affected  $t_d$  more than the uncertainty in  $V_{fw, on}$ .  $V_{fw, on}$  was estimated with an acceptable uncertainty for this study (figure 7), despite that most of the simulations did not simulate a groundwater salinity distribution which corresponds to the observed well depth distributions (figure 4). We therefore deem these simulations acceptable for this broad, general analysis, but

extra work would be required to analyze smaller scale groundwater salinity issues.

Finally, we would like to stress that for 9 out of 15 simulated deltas (figures 6 and 7), fresh groundwater volumes were formed over very long timescales. The fact that mankind currently already has the capacity to exhaust the fresh groundwater volumes for six of these (Nile, Pearl, Yangtze, Yellow River, Mekong, and Ganges-Brahmaputra), undoing thousands of years of natural development within three human life spans, is concerning. The fresh groundwater resources should be carefully managed in the deltas that have poor quality surface water, as replacing good quality groundwater with poor quality surface water reduces a delta's defenses from (future) water scarcity. Reducing groundwater extractions can pay off, as halving the total extracted groundwater often increases  $t_d$  by an order of magnitude (figure 7).

## Data availability statement

The data that support the findings of this study are openly available at the following URL/DOI: [10.5281/zenodo.6350503](https://doi.org/10.5281/zenodo.6350503).

## Acknowledgments

We thank Jaap Nienhuis for helping with the estimation of tidal factors and tidal intrusion length. Furthermore, we thank Philip Minderhoud and Liduin Burgering for providing the well extraction data of the Mekong and Rhine-Meuse delta respectively. In addition, we thank Joost Delsman for providing the salinity data of the Rhine-Meuse delta. Finally, we like to thank three anonymous reviewers for their aid in the improvement of this manuscript `delta_aquifer` (van Engelen 2022). This research has been supported by the Nederlandse Organisatie voor Wetenschappelijk Onderzoek (NWO) under the *New Delta* programme (Grant No. 869.15.013), and by Deltares' strategic research projects *Water Resources & Long-term Delta Developments*. Simulations were carried out on the Dutch national super computer Cartesius with the support of the SURF Cooperative, on an NWO Pilot Project Grant.

## Appendix A. Model description

Idealized models of 15 major deltas were created based on a set of 21 inputs, in order to conceptualize the deltas' geometry, lithology, hydrogeology, and boundary conditions. The model conceptualization was based on earlier work in van Engelen *et al* (2020), with two main differences. First, a full glacial cycle (125 ka) was simulated, starting from an initially saline groundwater system, instead of half a glacial cycle (40 ka) with an initially fresh groundwater system. Second, in this research, inputs were selected to create nine representative models (section A.4) for each delta, instead of the purely synthetic work in van Engelen *et al* (2020), which was required for the global sensitivity analysis in that study. The representative inputs are based on a literature study (section A.4), for which the values are listed in table A1. The next subsections will describe the creation of the models' components. A visual summary for all inputs that set spatial aspects of the model are summarized in figure A1.

### A.1. Geometry

First, a fan shaped delta was created by setting a total length ( $L$ ) and a sector angle ( $\varphi_f$ ) in the horizontal plane.  $L$  is subdivided in an onshore length ( $L_a$ ), i.e. the distance between delta apex to coastline, and an offshore length ( $L_b$ ), i.e. the distance between

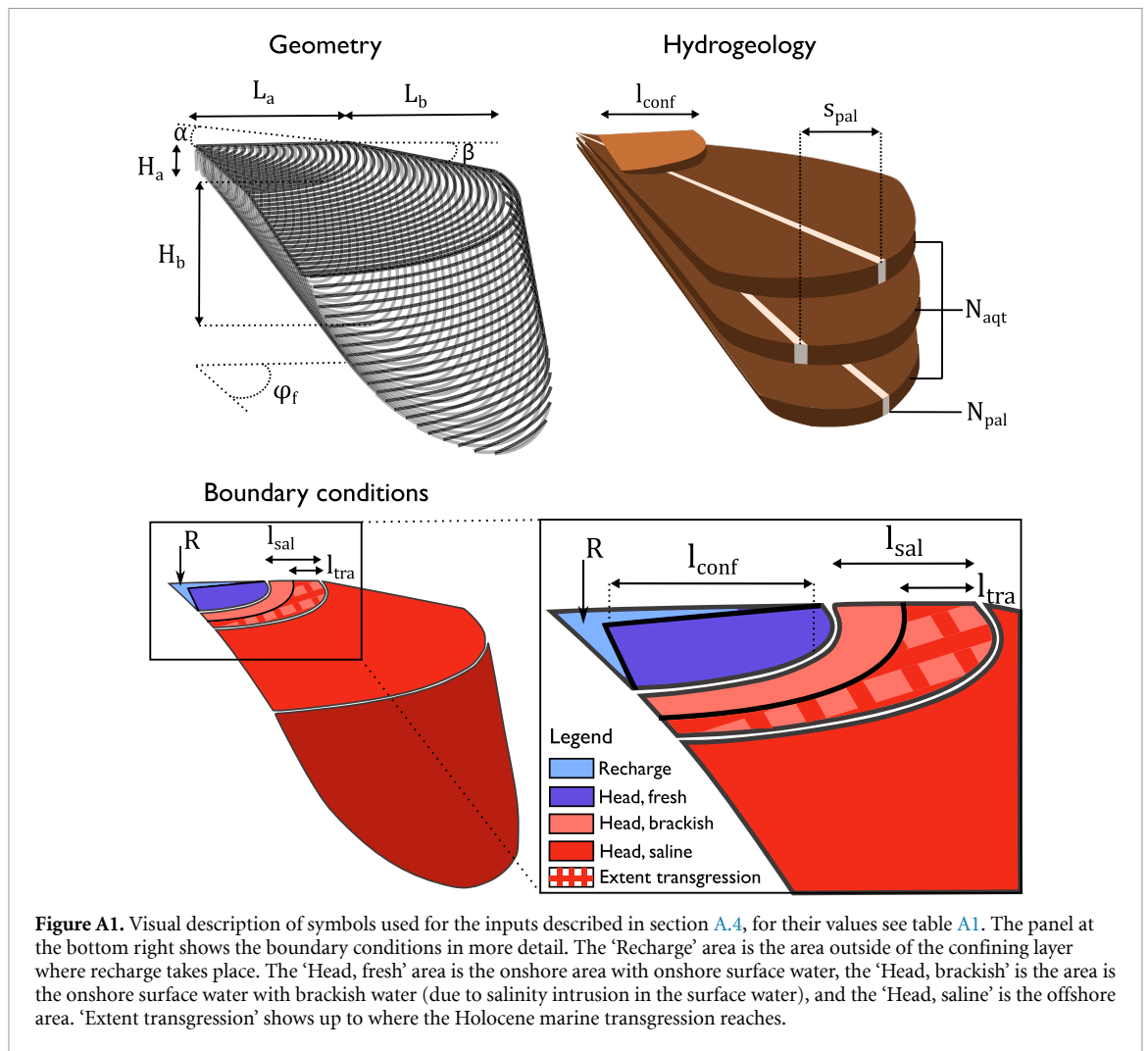
the coastline and the foot of the coastal slope. Therefore:  $L = L_a + L_b$ . The inputs  $\alpha$ ,  $\beta$ , and  $\gamma$  specify respectively the slope of the onshore part, the coastal shelf and coastal slope. Finally,  $H_a$  and  $H_b$  respectively set the depth of the aquifer at the delta apex and the center of the coastline. The hydrogeological base is conceptualized as a half-ellipsoid across the  $\varphi - z$  plane.

### A.2. Lithology and hydrogeology

The lithology was conceptualized deterministically. On top a confining layer was positioned, which from the coastline, reached up to  $l_{\text{conf}}$  the distance to the apex. Underneath the confining layer, a number  $N_{\text{aqt}}$  of aquitards were positioned. Each aquitard was incised by a number  $N_{\text{pal}}$  of straight paleochannels, at a relative distance  $s_{\text{pal}}$  from paleochannels in an overlying aquitard.  $f_{\text{aqt}}$  sets the relative thickness of clay in the sediment column. The hydrogeology was specified by setting the porosity ( $n$ ), the horizontal hydraulic conductivity of the aquifers ( $K_{\text{h,aqt}}$ ), the vertical hydraulic conductivity of the aquitards ( $K_{\text{v,aqt}}$ ), as these were the inputs usually provided in the literature, adhering to the main groundwater flow directions (Domenico and Schwartz 1990). These were converted to a  $K_{\text{v,aqt}}$  and a  $K_{\text{h,aqt}}$  with the anisotropy ( $K_{\text{h}}/K_{\text{v}}$ ). Deposition of the confining layer was simulated by converting the hydraulic conductivity of the cells in the confining layer from  $K_{\text{h,aqt}}$  to  $K_{\text{h,aqt}}$  during the marine regression. The longitudinal dispersivity  $a_l$  was fixed to 2 m, a representative value for regional models (Zech *et al* 2015). These were converted to a transversal dispersivity and vertical dispersivity by multiplying  $a_l$  with a factor 0.1 and 0.01 respectively (Zech *et al* 2015).

### A.3. Boundary conditions

We used the median out of the ensemble eustatic sea level derived by Spratt and Lisiecki (2016) of the last 125 ka to set the heads offshore and determine the coastline. The code used (iMOD-WQ), requires constant sea levels in stress periods, so each stress period was set to its mean sea level. We used stress-periods of 8000 years during the Pleistocene, and refined them starting from 11 ka, as during this period the sea started to rise very rapidly (figure 3(c)). A marine transgression was forced by  $t_{\text{tra}}$ , which is the time when the transgression reached its maximum extent, and  $l_{\text{tra}}$ , which is the part of the onshore length  $L_a$  covered by the transgression at maximum extent. Onshore surface water was conceptualized as a linear decreasing profile from the delta apex with constant height towards the coastline, which varied in height and location along with the sea level curve. Saline surface water intrusion in the surface water system was included as a linear salinity profile, which started at the concentration of sea water at the coastline,



and linearly decreased landwards to zero at  $l_{sal}$ . These boundary conditions together with the boundary conditions offshore consisted of assigned heads and assigned salinity of incoming fluxes. The area of the delta not covered by the confining layer received a natural groundwater recharge flux of infiltrated rainfall  $R$ , of which the magnitude varied through time. In reality, the groundwater recharge was very dynamic (Gossel *et al* 2010), so the constant recharge is a first-order approximation. We deemed this as sufficient, as a global sensitivity analysis published in van Engelen *et al* (2020), showed only a very limited sensitivity of  $V_{fw}$  to  $R$ .

#### A.4. Input data and parameterization

Our idealized models require a set of 21 inputs to create a geometry, lithology, hydrogeology, and boundary conditions. We conducted a literature study to obtain representative inputs for 15 deltas, of which the values can be found in table A1 and the literature sources can be found in table A2. Parameters to specify lateral geometry, the topography, and bathymetry were determined from global datasets

(Syvitski and Saito 2007, Weatherall *et al* 2015, Kulp and Strauss 2019). Groundwater system thicknesses were, if available, retrieved from case studies, or, if not, from the global aquifer system thickness estimation dataset (Zamrsky *et al* 2018). The lithological inputs were retrieved purely from local studies (table A2), as no global dataset of groundwater system interiors exist. No lithological data could be found for the Tokar delta (Sudan), so here we used the median value of each lithological input across all deltas in our dataset. The boundary condition inputs (salinity intrusion length and marine transgression) were also retrieved from local studies, except for the cases where no data could be found for the salinity intrusion length in the surface water system (The Tokar, Kelantan, and Burdekin delta). A comparison with a global dataset of the tidal factor and tidal intrusion length (Nienhuis *et al* 2020) confirmed that saline water intrusion is presumably not occurring in these deltas and could be set to zero. For the hydrogeologic inputs, input ranges were usually provided in the local studies. Based on a global sensitivity analysis (van Engelen *et al* 2020), we varied the inputs that

**Table A1.** The inputs for all 15 deltas, based on a literature study (see table A2). For an explanation of the symbols, see figure A1. Inputs in cursive were values filled with the median value across 30 deltas.

Delta	$L_a$ (km)	$L_b$ (km)	$\alpha$ (rad)	$\beta$ (rad)	$H_a$ (m)	$H_b$ (m)	$\varphi_f$ ( $\pi$ rad)	$N_{\text{aqt}}$ (—)	$f_{\text{aqt}}$ (—)	$l_{\text{conf}}$ (—)
Burdekin	32	130	$5.0 \times 10^{-4}$	$6.7 \times 10^{-4}$	10	100	0.6	2	0.6	1
Chao Praya	164	200	$3.0 \times 10^{-5}$	$1.3 \times 10^{-4}$	300	600	0.18	7	0.5	1
Ganges- Brahmaputra	335	200	$9.0 \times 10^{-5}$	$5.0 \times 10^{-4}$	250	500	0.31	50	0.75	1
Kelantan	35	200	$2.5 \times 10^{-4}$	$2.0 \times 10^{-4}$	50	250	0.29	2	0.2	1
Mekong	232	200	$3.0 \times 10^{-5}$	$4.3 \times 10^{-4}$	250	500	0.32	8	0.4	1
Mississippi	197	180	$2.0 \times 10^{-5}$	$1.5 \times 10^{-3}$	600	1000	0.33	30	0.5	1
Nile	175	46	$9.0 \times 10^{-5}$	$2.0 \times 10^{-3}$	200	1000	0.33	4	0.4	1
Pearl	106	200	$2.9 \times 10^{-5}$	$1.0 \times 10^{-3}$	15	50	0.16	1	0.9	1
Po	56	200	$4.0 \times 10^{-5}$	$4.0 \times 10^{-4}$	300	1000	0.41	10	0.5	0
Red River	136	200	$5.0 \times 10^{-5}$	$3.5 \times 10^{-4}$	40	150	0.26	1	0.3	1
Rhine-Meuse	131	200	$7.5 \times 10^{-5}$	$1.7 \times 10^{-4}$	180	280	0.28	3	0.1	1
Saloum	73	32	$4.2 \times 10^{-5}$	$2.6 \times 10^{-3}$	80	80	0.18	1	0.1	0
Tokar	45	73	$1.1 \times 10^{-3}$	$4.0 \times 10^{-3}$	50	250	0.36	2	0.5	0.3
Yangtze	215	200	$6.0 \times 10^{-5}$	$3.0 \times 10^{-4}$	50	250	0.24	4	0.5	1
Yellow River	181	200	$1.0 \times 10^{-3}$	$1.5 \times 10^{-4}$	30	300	0.26	5	0.2	0.6

Delta	$N_{\text{pal}}$ (—)	$s_{\text{pal}}$ (—)	$K_{\text{h,aqf}}$ ( $\text{m d}^{-1}$ )	$K_{\text{v,aqt}}$ ( $\text{m d}^{-1}$ )	$K_{\text{h}}/K_{\text{v}}$ (—)	$n$ (—)	$l_{\text{tra}}$ (—)	$t_{\text{tra}}$ (ka)	$N_{\text{chan}}$ (—)	$l_{\text{sal}}$ (—)	$R$ ( $\text{m d}^{-1}$ )
Burdekin	2	0.6	10.0–200.0	$7.8 \times 10^{-6}$ – $1.5 \times 10^{-1}$	1	0.3	1	10	2	0	$2.55 \times 10^{-4}$
Chao Praya	2	0.6	3.7–120.0	$2.1 \times 10^{-7}$ – $5.0 \times 10^{-4}$	10	0.3	0.7	6	1	0.36	$9.78 \times 10^{-5}$
Ganges- Brahmaputra	30	0.6	17.3–69.1	$8.6 \times 10^{-4}$ – $7.8 \times 10^{-3}$	10	0.3	0.1	7	4	0.55	$6.13 \times 10^{-4}$
Kelantan	2	0.6	$8.6 \times 10^{-4}$ –8.64	$7.8 \times 10^{-6}$ – $1.5 \times 10^{-1}$	10	0.3	0.25	6	1	0	$2.90 \times 10^{-4}$
Mekong	2	0.6	0.518–67.5	$5.2 \times 10^{-6}$ – $8.6 \times 10^{-2}$	3	0.3	1	8	4	0.18	$6.36 \times 10^{-4}$
Mississippi	2	0.6	0.3–114.0	$4.0 \times 10^{-3}$ – $4.0 \times 10^{-2}$	10	0.3	1	8	1	0	$2.90 \times 10^{-4}$
Nile	2	0.6	6.6–100.0	$1.0 \times 10^{-5}$ – $6.6 \times 10^{-1}$	32	0.3	0.15	8	2	0	0.0
Pearl	2	0.6	1.0–30.0	$8.6 \times 10^{-6}$ – $1.0 \times 10^{-3}$	10	0.3	0.8	6.8	5	0.34	$2.74 \times 10^{-4}$
Po	2	0.6	0.0864–86.4	$8.6 \times 10^{-6}$ – $8.6 \times 10^{-4}$	10	0.3	0.43	6	1	0	$4.24 \times 10^{-4}$
Red River	2	0.6	4.92–29.4	$8.6 \times 10^{-7}$ – $8.6 \times 10^{-3}$	10	0.2	0.8	9	3	0.08	$2.90 \times 10^{-4}$
Rhine-Meuse	4	0.2	0.1–100.0	$1.0 \times 10^{-3}$ – $1.0 \times 10^{-1}$	10	0.3	0.2	7.5	2	0.27	$5.00 \times 10^{-4}$
Saloum	2	0.6	1.47–190.0	$7.8 \times 10^{-6}$ – $1.5 \times 10^{-1}$	10	0.3	0.9	4.5	2	1.67	0.0
Tokar	2	0.6	1.79–42.2	$7.8 \times 10^{-6}$ – $1.5 \times 10^{-1}$	10	0.3	0.75	6	1	0	$4.11 \times 10^{-5}$
Yangtze	2	0.6	4.0–15.0	$1.0 \times 10^{-6}$ – $2.0 \times 10^{-5}$	10	0.3	1	7	1	0.12	$2.90 \times 10^{-4}$
Yellow River	2	0.6	1.8–200.0	$1.8 \times 10^{-4}$ – $2.0 \times 10^{-2}$	10	0.3	0.2	6	1	0	$2.90 \times 10^{-4}$

create the most output uncertainty, namely the horizontal hydraulic conductivity in the aquifers ( $K_{\text{h,aqf}}$ ) and the vertical hydraulic conductivity of the aquitard ( $K_{\text{v,aqt}}$ ). If no input range was available for  $K_{\text{h,aqf}}$  in a delta, a data range was taken from a global permeability dataset (Huscroft *et al* 2018), which provided a wide range that varies roughly three orders of magnitude. If no input range could be found for  $K_{\text{v,aqt}}$  in a delta, an input range was created by taking the logarithmic mean of the minimum and maximum

values for  $K_{\text{v,aqt}}$  across all deltas. We discretized the input range of  $K_{\text{h,aqf}}$  and  $K_{\text{h,aqt}}$  in three levels (minimum, logarithmic mean and maximum), and conducted a full factorial analysis for each delta. This resulted in nine simulations per delta. The other hydrogeologic inputs were averaged over their reported range, which were the porosity, infiltration recharge, and the formation anisotropy. If data was missing for one of these four inputs for a delta, the median value of all deltas was assigned.

Table A2. Literature used to obtain the inputs in table A1.

Delta	Geometry	Lithology	Hydrogeology	Boundary conditions
Burdekin	Mcmahon <i>et al</i> (2000), Fass <i>et al</i> (2007)	Mcmahon <i>et al</i> (2000)	Mcmahon <i>et al</i> (2000), Narayan <i>et al</i> (2007)	Fielding <i>et al</i> (2006), Nienhuis <i>et al</i> (2020)
Chao Praya	Sanford and Buapeng (1996), Yamanaka <i>et al</i> (2011)	Sanford and Buapeng (1996), Yamanaka <i>et al</i> (2011)	Das Gupta (1985), Giao <i>et al</i> (1998)	Sinsakul (2000), Savenije (2012)
Ganges-Brahmaptura	Bonsor <i>et al</i> (2017)	Michael and Voss (2009b), Bonsor <i>et al</i> (2017)	Michael and Voss (2009b)	Goodbred and Kuehl (2000), Shamsudduha and Uddin (2007)
Kelantan	Sefie <i>et al</i> (2018)	Samsudin <i>et al</i> (1997, 2008)	Huscroft <i>et al</i> (2018)	Tilmans (1991), Nienhuis <i>et al</i> (2020)
Mekong	Minderhoud <i>et al</i> (2017), Van Pham <i>et al</i> (2019)	Minderhoud <i>et al</i> (2017), Van Pham <i>et al</i> (2019)	Minderhoud <i>et al</i> (2017), Van Pham <i>et al</i> (2019)	Nguyen and Savenije (2006), Tamura <i>et al</i> (2009)
Mississippi	Griffith (2003)	Griffith (2003)	Griffith (2003), Thompson <i>et al</i> (2007)	Coleman <i>et al</i> (1998), Nienhuis <i>et al</i> (2020)
Nile	Sestini (1989)	van Engelen <i>et al</i> (2019)	Kashef (1983), van Engelen <i>et al</i> (2019)	Stanley and Warne (1993), Pennington <i>et al</i> (2017), Nienhuis <i>et al</i> (2020)
Pearl	Wang and Jiao (2012), Zong <i>et al</i> (2012)	Wang and Jiao (2012), Zong <i>et al</i> (2012)	Yang <i>et al</i> (2013), Kwong and Jiao (2016)	Zong <i>et al</i> (2009), Zhang <i>et al</i> (2013)
Po	Teatini <i>et al</i> (2011)	Teatini <i>et al</i> (2011), Colombani <i>et al</i> (2017)	Teatini <i>et al</i> (2011), Colombani <i>et al</i> (2016)	Amorosi and Colalongo (2005), Nienhuis <i>et al</i> (2020)
Red River	Winkel <i>et al</i> (2011), Larsen <i>et al</i> (2017)	Winkel <i>et al</i> (2011), Larsen <i>et al</i> (2017)	Larsen <i>et al</i> (2017)	Ca <i>et al</i> (1994), Tanabe <i>et al</i> (2006)
Rhine-Meuse	Hummelman <i>et al</i> (2019)	Hummelman <i>et al</i> (2019)	Oude Essink <i>et al</i> (2010), De Lange <i>et al</i> (2014)	Peelen (1970), de Haas <i>et al</i> (2018)
Saloum	Faye <i>et al</i> (2005)	Faye <i>et al</i> (2005)	Faye <i>et al</i> (2005)	Ausseil-Badie <i>et al</i> (1991), Nienhuis <i>et al</i> (2020)
Tokar	Zamrsky <i>et al</i> (2018)	No Data	Hussein (1982)	Nienhuis <i>et al</i> (2020)
Yangtze	Xue <i>et al</i> (2008), Shi <i>et al</i> (2012)	Xue <i>et al</i> (2008), Shi <i>et al</i> (2012)	Chen <i>et al</i> (2014)	Saito <i>et al</i> (2001), Wu and Zhu (2010)
Yellow River	Han <i>et al</i> (2011)	Han <i>et al</i> (2011)	Cao <i>et al</i> (2016)	Saito <i>et al</i> (2001)

**Appendix B. Risk map**

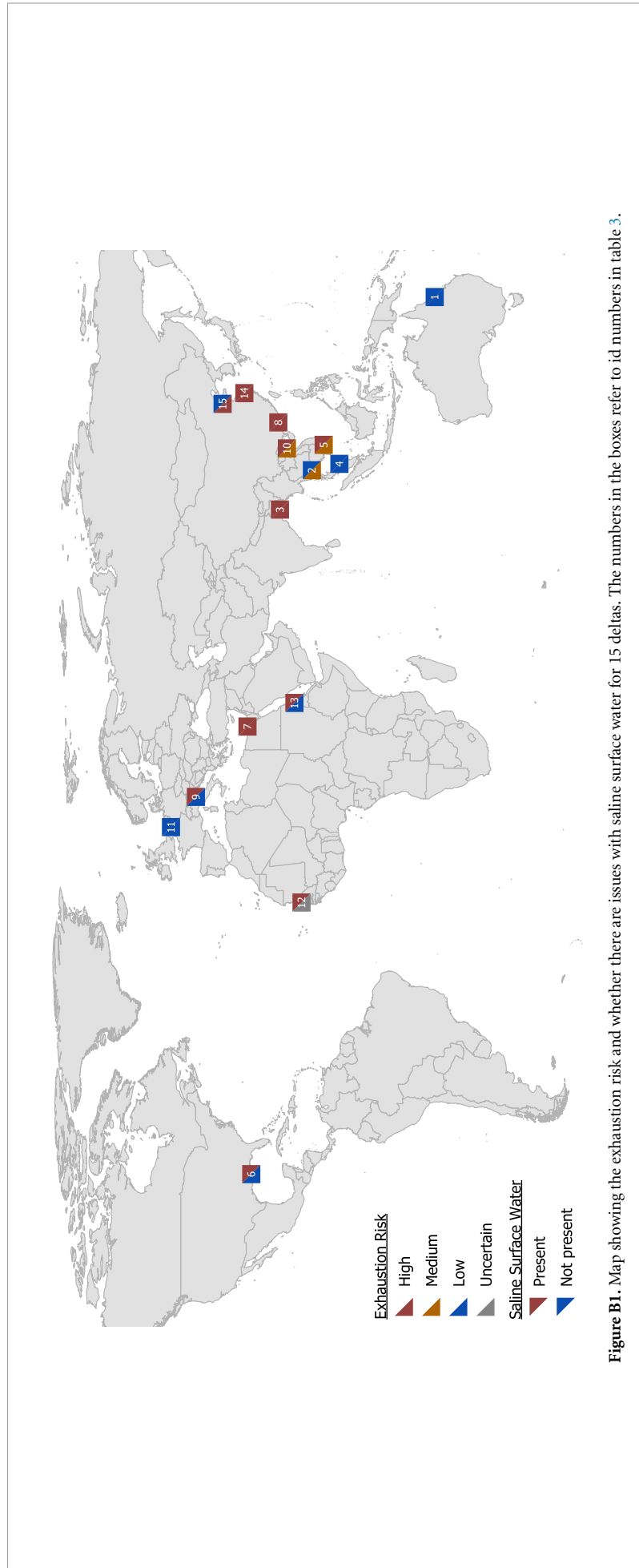


Figure B1. Map showing the exhaustion risk and whether there are issues with saline surface water for 15 deltas. The numbers in the boxes refer to id numbers in table 3.

## ORCID iDs

J van Engelen  <https://orcid.org/0000-0002-7628-2548>

G H P Oude Essink  <https://orcid.org/0000-0003-0931-6944>

M F P Bierkens  <https://orcid.org/0000-0002-7411-6562>

## References

- Akouvi A, Dray M, Violette S, de Marsily G and Zuppi G M 2008 The sedimentary coastal basin of Togo: example of a multilayered aquifer still influenced by a palaeo-seawater intrusion *Hydrogeol. J.* **16** 419–36
- Al Nahian M, Ahmed A, Lázár A N, Hutton C W, Salehin M and Streatfield P K 2018 Drinking water salinity associated health crisis in coastal Bangladesh *Elementa* **6** 1–14
- Allen J R 1964 Sedimentation in the modern delta of the River Niger, West Africa *Dev. Sedimentol.* **1** 26–34
- Amorosi A and Colalongo M L 2005 The linkage between alluvial and coeval nearshore marine successions: evidence from the late quaternary record of the PO River Plain, Italy *Fluvial Sedimentology VII* ed M D Blum, S B Marriot and S F Leclair (Malden: Blackwell Publishing) pp 255–75
- Anderson W, Lorenzo-Trueba J and Voller V 2019 A geomorphic enthalpy method: description and application to the evolution of fluvial-deltas under sea-level cycles *Comput. Geosci.* **130** 1–10
- Anthony E J 1995 Beach-ridge development and sediment supply: examples from West Africa *Mar. Geol.* **129** 175–86
- Ausseil-Badie J, Barousseau J P, Descamps C, Salif Diop E H, Giresse P and Pazdur M 1991 Holocene deltaic sequence in the Saloum Estuary, Senegal *Quat. Res.* **36** 178–94
- Ayers J C, Goodbred S, George G, Fry D, Benneyworth L, Hornberger G, Roy K, Karim M R and Akter F 2016 Sources of salinity and arsenic in groundwater in southwest Bangladesh *Geochem. Trans.* **17** 1–22
- Behera A K, Chakrapani G J, Kumar S and Rai N 2019 Identification of seawater intrusion signatures through geochemical evolution of groundwater: a case study based on coastal region of the Mahanadi delta, Bay of Bengal, India *Nat. Hazards* **97** 1209–30
- Biswas A K 1993 Land resources for sustainable agricultural development in Egypt *Ambio* **22** 556–60
- Bonsor H C *et al* 2017 Hydrogeological typologies of the Indo-Gangetic basin alluvial aquifer, South Asia *Hydrogeol. J.* **25** 1377–406
- Bording T, Christiansen A V, Auken E, Gunnink J and Oude Essink G H 2017 Groundbased TEM survey in the subsiding mekong delta *23rd European Meeting of Environmental and Engineering Geophysics* pp 2015–8
- Bredehoeft J 2002 The water budget myth revisited: why hydrogeologists model *Groundwater* **40** 340–5
- Bucx T, Marchand M, Makaske B and van de Guchte C 2010 Comparative assessment of the vulnerability and resilience of 10 deltas—synthesis report *Technical Report* (Delta Alliance International, Delft-Wageningen)
- Ca V T, Vongvisessomjai S and Asaeda T 1994 Study on salinity intrusion in the Red River Delta *Environ. Syst. Res.* **22** 213–8
- Cao G, Han D, Currell M J and Zheng C 2016 Revised conceptualization of the North China Basin groundwater flow system: groundwater age, heat and flow simulations *J. Asian Earth Sci.* **127** 119–36
- Chen J, Taniguchi M, Liu G, Miyaoka K, Onodera S I, Tokunaga T and Fukushima Y 2007 Nitrate pollution of groundwater in the Yellow River delta, China *Hydrogeol. J.* **15** 1605–14
- Chen X X, Luo Z J and Zhou S L 2014 Influences of soil hydraulic and mechanical parameters on land subsidence and ground fissures caused by groundwater exploitation *J. Hydrodyn.* **26** 155–64
- Chen Z, Chen Z and Zhang W 1997 Quaternary stratigraphy and trace-element indices of the Yangtze Delta, Eastern China, with special reference to marine transgressions *Quat. Res.* **47** 181–91
- Coleman J M, Roberts H H and Stone G W 1998 Mississippi River delta: an overview *J. Coast. Res.* **14** 698–716
- Coleman J and Huh O 2003 Major deltas of the world: a perspective from space *Technical Report* (Baton Rouge, LA: Coastal Studies Institute, Louisiana State University)
- Colombani N, Cuoco E and Mastrocicco M 2017 Origin and pattern of salinization in the Holocene aquifer of the southern Po Delta (NE Italy) *J. Geochem. Explor.* **175** 130–7
- Colombani N, Osti A, Volta G and Mastrocicco M 2016 Impact of climate change on salinization of coastal water resources *Water Resour. Manage.* **30** 2483–96
- Cooke G A 1985 Reconstruction of the Mesopotamian coastline in the Holocene *Geol. Soc. Am. Abstr.* **2** 15–28
- Dai Z, Chu A, Stive M, Zhang X and Yan H 2011 Unusual salinity conditions in the Yangtze Estuary in 2006: impacts of an extreme drought or of the three gorges dam? *Ambio* **40** 496–505
- Das Gupta A 1985 Simulated salt-water movement in the Nakhon Luang Aquifer, Bangkok, Thailand *Groundwater* **23** 512–22
- Davis A, Lewis S, O'Brien D, Bainbridge Z, Bentley C, Mueller J and Brodie J 2014 Water resource development and high value coastal wetlands on the Lower Burdekin Floodplain, Australia *Estuaries of Australia in 2050 and Beyond* ed E Wolanski (Dordrecht: Springer) ch 13, pp 223–45
- de Haas T, Pierik H J, van der Spek A J, Cohen K M, van Maanen B and Kleinhans M G 2018 Holocene evolution of tidal systems in The Netherlands: effects of rivers, coastal boundary conditions, eco-engineering species, inherited relief and human interference *Earth-Sci. Rev.* **177** 139–63
- De Lange W J *et al* 2014 An operational, multi-scale, multi-model system for consensus-based, integrated water management and policy analysis: The Netherlands Hydrological Instrument *Environ. Modelling Softw.* **59** 98–108
- de Montety V, Radakovitch O, Vallet-Coulomb C, Blavoux B and Travi Y 2008 Geochemical evolution and timescale of seawater intrusion in a confined coastal aquifer: case of the Rhone Delta *13th IWRA World Water Congress (Montpellier, 1–4 September 2008)*
- Delsman J R, Hu-a-ng K R M, Vos P C, De Louw P G B, Oude Essink G H P, Stuyfzand P J and Bierkens M F P 2014 Paleo-modeling of coastal saltwater intrusion during the Holocene: an application to the Netherlands *Hydrol. Earth Syst. Sci.* **18** 3891–905
- Delsman J R, Oude Essink G H, Huizer S, Bootsma H, Mulder T, Zitman P and Romero Verastegui B 2020 Actualisatie zout in het NHI—toolbox NHI zoet-zout modellering en landelijk model *Technical Report* (Utrecht: Deltares)
- Delsman J *et al* 2018 Large-scale, probabilistic salinity mapping using airborne electromagnetics for groundwater management in Zeeland, the Netherlands *Environ. Res. Lett.* **13** 084011
- Dieng N M, Orban P, Otten J, Stumpp C, Faye S and Dassargues A 2017 Temporal changes in groundwater quality of the Saloum coastal aquifer *J. Hydrol.: Reg. Stud.* **9** 163–82
- Dirks F J H, Rismianto D and De Wit G J 1989 Groundwater in Bekasi District, West Java, Indonesia *Nat. Tijdschr.* **70** 47–55
- Domenico P and Schwartz F W 1990 *Physical and Chemical Hydrogeology* 1st edn (Toronto: Wiley)
- Edmunds W M 2001 Palaeowaters in European coastal aquifers—the goals and main conclusions of the PALAEAUX project *Geol. Soc. London Spec. Publ.* **189** 1–16
- El-Agha D E, Closas A and Molle F 2017 Below the radar: the boom of groundwater use in the central part of the Nile Delta in Egypt *Hydrogeol. J.* **25** 1621–31

- Elkral A B and Obied B A 2013 Hydrochemical leftacterization and groundwater quality in Delta Tokar alluvial plain, Red Sea coast-Sudan *Arab. J. Geosci.* **6** 3133–8
- Ericson J P, Vörösmarty C J, Dingman S L, Ward L G and Meybeck M 2006 Effective sea-level rise and deltas: causes of change and human dimension implications *Glob. Planet. Change* **50** 63–82
- Eslami S et al 2021 Projections of salt intrusion in a mega-delta under climatic and anthropogenic stressors *Commun. Earth Environ.* **2** 1–11
- Fan X, Pedroli B, Liu G, Liu Q, Liu H and Shu L 2012 Soil salinity development in the yellow river delta in relation to groundwater dynamics *Land Degrad. Dev.* **23** 175–89
- Fass T, Cook P G, Stieglitz T and Herczeg A L 2007 Development of saline ground water through transpiration of sea water *Ground Water* **45** 703–10
- Faye S, Maloszewski P, Stichler W, Trimborn P, Faye S C and Gaye C B 2005 Groundwater salinization in the Saloum (Senegal) delta aquifer: minor elements and isotopic indicators *Sci. Total Environ.* **343** 243–59
- Fielding C R, Trueman J D and Alexander J 2006 Holocene depositional history of the Burdekin River Delta of northeastern Australia: a model for a low-accommodation, highstand delta *J. Sediment. Res.* **76** 411–28
- Geirnaert W and Laeven M P 1992 Composition and history of ground water in the western Nile Delta *J. Hydrol.* **138** 169–89
- Geriesh M H, Balke K-D, El-Rayes A E and Mansour B M 2015 Implications of climate change on the groundwater flow regime and geochemistry of the Nile Delta, Egypt *J. Coast. Conserv.* **19** 589–608
- Giambastiani B M, Colombani N, Mastrociccio M and Fidelibus M D 2013 Characterization of the lowland coastal aquifer of Comacchio (Ferrara, Italy): hydrology, hydrochemistry and evolution of the system *J. Hydrol.* **501** 35–44
- Giao P H, Phien-Wej N and Honjo Y 1998 FEM quasi-3D modelling of responses to artificial recharge in the Bangkok multiaquifer system *Environ. Modelling Softw.* **14** 141–51
- Giosan L et al 2018 On the Holocene evolution of the Ayeyawady megadelta *Earth Surf. Dyn.* **6** 451–66
- Giosan L, Syvitski J, Constantinescu S and Day J 2014 Climate change: protect the world's deltas *Nature* **516** 31–33
- Goodbred S L and Kuehl S A 2000 The significance of large sediment supply, active tectonism and eustasy on margin sequence development: late quaternary stratigraphy and evolution of the Ganges-Brahmaputra delta *Sediment. Geol.* **133** 227–48
- Gossel W, Sefelnasr A and Wycisk P 2010 Modelling of paleo-saltwater intrusion in the northern part of the Nubian Aquifer System, Northeast Africa *Hydrogeol. J.* **18** 1447–63
- Griffith J M 2003 *Hydrogeologic Framework of Southeastern Louisiana* 72 USGS
- Gunnink J, Pham H V, Oude Essink G and Bierkens M 2021 The 3D groundwater salinity distribution and fresh groundwater volumes in the Mekong Delta, Vietnam, inferred from geostatistical analyses *Earth Syst. Sci. Data Discuss.* **4441776** 1–31
- Han D, Kohfahl C, Song X, Xiao G and Yang J 2011 Geochemical and isotopic evidence for palaeo-seawater intrusion into the south coast aquifer of Laizhou Bay, China *Appl. Geochem.* **26** 863–83
- Hehanussa P E 1980 Appendix 2: excursion guide to the Cimanuk Delta complex, west Java *Proc. Jakarta Workshop on Coastal Resources Management*
- Hoang H T T et al 2018 Impact of anthropogenic activities on water quality and plankton communities in the Day River (Red River Delta, Vietnam) *Environ. Monit. Assess.* **190** 67
- Hummelman J, Maljers D, Menkovic A, Reindersma R, Vermes R and Stafleu J 2019 Totstandkomingsrapport hydrogeologisch model (REGIS II v2.2) *Technical Report* (Utrecht: Netherlands Institute of Applied Geoscience TNO)
- Huscroft J, Gleeson T, Hartmann J and Börker J 2018 Compiling and mapping global permeability of the unconsolidated and consolidated earth: GLobal HYdrogeology MaPS 2.0 (GLHYMPS 2.0) *Geophys. Res. Lett.* **45** 1897–904
- Hussein M T 1982 Evaluation of groundwater resources in Tokar Delta, Sudan *Hydrol. Sci. J.* **27** 139–45
- Jakovovic D, Werner A D, de Louw P G, Post V E and Morgan L K 2016 Saltwater upconing zone of influence *Adv. Water Resour.* **94** 75–86
- Kashef A-A I 1983 Salt-water intrusion in the Nile Delta *Groundwater* **21** 160–7
- Khan A E, Scheelbeek P F D, Shilpi A B, Chan Q, Mojumder S K, Rahman A, Haines A and Vineis P 2014 Salinity in drinking water and the risk of (pre)eclampsia and gestational hypertension in coastal Bangladesh: a case-control study *PLoS One* **9** e108715
- Kooi H, Groen J and Leijnse A 2000 Modes of seawater intrusion during transgressions *Water Resour. Res.* **36** 3581–9
- Kooy M, Walter C T and Prabaharyaka I 2016 Inclusive development of urban water services in Jakarta: the role of groundwater *Habitat Int.* **73** 109–18
- Kozerski B 1983 Problems of the salt water origin in the Vistula delta aquifers *Proc. 8th Salt Water Intrusion Meeting (Bari, Italy)* pp 325–34
- Kulp S A and Strauss B H 2019 New elevation data triple estimates of global vulnerability to sea-level rise and coastal flooding *Nat. Commun.* **10** 4844
- Kwong H T and Jiao J J 2016 Hydrochemical reactions and origin of offshore relatively fresh pore water from core samples in Hong Kong *J. Hydrol.* **537** 283–96
- Larsen F, Tran L V, Van Hoang H, Tran L T, Christiansen A V and Pham N Q 2017 Groundwater salinity influenced by Holocene seawater trapped in incised valleys in the Red River delta plain *Nat. Geosci.* **10** 376–82
- LGWRC 2012 *Managing Louisiana's groundwater resources Technical Report* (Baton Rouge, LA: Louisiana Ground Water Resources Commission Commission)
- LPHI and AAE 2016 *Groundwater for power plants: a big risk to New Orleans East Technical Report* (New Orleans, LA: Louisiana Public Health Institute)
- Lu C, Kitanidis P K and Luo J 2009 Effects of kinetic mass transfer and transient flow conditions on widening mixing zones in coastal aquifers *Water Resour. Res.* **45** 1–17
- Mabrouk M, Jonoski A, Oude Essink G H and Uhlenbrook S 2018 Impacts of sea level rise and increasing fresh water demand on sustainable groundwater management *Water* **10** 1–14
- Manzano M, Custodio E, Loosli H, Cabrera M C, Riera X and Custodio J 2001 Palaeowater in coastal aquifers of Spain *Geol. Soc. London Spec. Publ.* **189** 107–38
- Mcmahon G A, Arunakumaren N J and Bajracharya K 2000 Hydrogeological conceptualisation of the Burdekin river delta *Proc. 3rd Int. Hydrology and Water Resources Symp. Institution of Engineers (Perth, Western Australia, Australia)*
- Meyer R, Engesgaard P and Sonnenborg T O 2019 Origin and dynamics of saltwater intrusion in a regional aquifer: combining 3-D saltwater modeling with geophysical and geochemical data *Water Resour. Res.* **55** 1792–813
- Michael H A, Post V E, Wilson A M and Werner A D 2017 Science, society and the coastal groundwater squeeze *Water Resour. Res.* **53** 2610–7
- Michael H A and Voss C I 2009a Controls on groundwater flow in the Bengal Basin of India and Bangladesh: Regional modeling analysis *Hydrogeol. J.* **17** 1561–77
- Michael H A and Voss C I 2009b Estimation of regional-scale groundwater flow properties in the Bengal Basin of India and Bangladesh *Hydrogeol. J.* **17** 1329–46
- Minderhoud P S J, Erkens G, Pham V, Bui V, Erban L, Kooi H and Stouthamer E 2017 Impacts of 25 years of groundwater extraction on subsidence in the Mekong delta, Vietnam *Environ. Res. Lett.* **12** 064006

- Narayan K A, Schleeberger C and Bristow K L 2007 Modelling seawater intrusion in the Burdekin Delta Irrigation Area, North Queensland, Australia *Agric. Water Manage.* **89** 217–28
- Naseem S, Husain V and Bano S 2018 Origin of salinity and other constituents in Indus deltaic plain groundwater, Thatta District, Pakistan *J. Coast. Res.* **344** 883–91
- Naus F L, Schot P, Groen K, Matin Ahmed K and Griffioen J 2019 Groundwater salinity variation in Upazila Assasuni (southwestern Bangladesh), as steered by surface clay layer thickness, relative elevation and present-day land use *Hydrol. Earth Syst. Sci.* **23** 1431–51
- Neumann B, Vafeidis A T, Zimmermann J and Nicholls R J 2015 Future coastal population growth and exposure to sea-level rise and coastal flooding—a global assessment *PLoS One* **10** e0118571
- Nguyen A D and Savenije H H G 2006 Salt intrusion in multi-channel estuaries: a case study in the Mekong Delta, Vietnam *Hydrol. Earth Syst. Sci.* **10** 743–54
- Nienhuis J H, Ashton A D, Edmonds D A, Hoitink A, Kettner A J, Rowland J C and Tornqvist T E 2020 Global-scale human impact on delta morphology has led to net land area gain *Nature* **577** 514–8
- Nogueira G, Stigter T Y, Zhou Y, Mussa F and Juizo D 2019 Understanding groundwater salinization mechanisms to secure freshwater resources in the water-scarce city of Maputo, Mozambique *Sci. Total Environ.* **661** 723–36
- Oude Essink G H 2001 Improving fresh groundwater supply—problems and solutions *Ocean Coast. Manage.* **44** 429–49
- Oude Essink G H, Van Baaren E S and De Louw P G 2010 Effects of climate change on coastal groundwater systems: a modeling study in the Netherlands *Water Resour. Res.* **46** 1–16
- Pauw P S, van der Zee S E A T M, Leijnse A and Oude Essink G H P 2015 Saltwater upconing due to cyclic pumping by horizontal wells in freshwater lenses *Groundwater* **54** 521–31
- Peelen R 1970 Changes in salinity in the delta area of the rivers Rhine and Meuse resulting from the construction of a number of enclosing Dams *Netherlands J. Sea Res.* **5** 1–19
- Pellenburg N P 1997 Groundwater management in The Netherlands: background and legislation *ILRA Workshop Groundwater Management (March 1984)* pp 137–49
- Pennington B T, Sturt F, Wilson P, Rowland J and Brown A G 2017 The fluvial evolution of the Holocene Nile Delta *Quat. Sci. Rev.* **170** 212–31
- Perrone D and Jasechko S 2017 Dry groundwater wells in the western United States *Environ. Res. Lett.* **12** 104002
- Post V E, Vandenbohede A, Werner A D, Maimun S and Teubner M D 2013 Groundwater ages in coastal aquifers *Adv. Water Resour.* **57** 1–11
- Prabaharan S, Lakshumanan C and Subramani T 2018 Geomorphic anomalies and natural resource of Krishna Godavari Basin using remote sensing techniques *Int. J. Earth Sci. Eng.* **11** 35–40
- QGIS Development Team 2021 QGIS Geographic Information System (Retrieved 01 October 2021)
- Rahman M M *et al* 2019 Salinization in large river deltas: drivers, impacts and socio-hydrological feedbacks *Water Secur.* **6** 100024
- Rasmussen E K, Svenstrup Petersen O, Thompson J R, Flower R J and Ahmed M H 2009 Hydrodynamic-ecological model analyses of the water quality of Lake Manzala (Nile Delta, Northern Egypt) *Hydrobiologia* **622** 195–220
- Saito Y, Yang Z and Hori K 2001 The Huanghe Yellow River and Changjiang Yangtze River deltas: a review on their characteristics, evolution and sediment discharge during the Holocene *Geomorphology* **41** 219–31
- Salman G and Abdula I 1995 Development of the Mozambique and Ruvuma sedimentary basins, offshore Mozambique *Sediment. Geol.* **96** 7–41
- Samsudin A R, Hamzah U and Rafek G 1997 Salinity study of coastal groundwater aquifers in north Kelantan, Malaysia *Abbiual Geological Conf.* '97
- Samsudin A R, Haryono A, Hamzah U and Rafek A G 2008 Salinity mapping of coastal groundwater aquifers using hydrogeochemical and geophysical methods: a case study from north Kelantan, Malaysia *Environ. Geol.* **55** 1737–43
- Sanford W E and Buapeng S 1996 Assessment of a groundwater flow model of the Bangkok Basin, Thailand *Hydrogeol. J.* **4** 26–40
- Santucci L, Carol E and Kruse E 2016 Identification of palaeo-seawater intrusion in groundwater using minor ions in a semi-confined aquifer of the Río de la Plata littoral (Argentina) *Sci. Total Environ.* **566–567** 1640–8
- Sarker M M R, Van Camp M, Islam M, Ahmed N and Walraevens K 2018 Hydrochemistry in coastal aquifer of southwest Bangladesh: origin of salinity *Environ. Earth Sci.* **77** 1–20
- Savenije H 2012 Salinity and tides in alluvial estuaries p 163 (available at: [www.lavoisier.fr/livre/notice.asp?ouvrage=1330707](http://www.lavoisier.fr/livre/notice.asp?ouvrage=1330707))
- Sefie A, Aris A Z, Ramli M F, Narany T S, Shamsuddin M K N, Saadudin S B and Zali M A 2018 Hydrogeochemistry and groundwater quality assessment of the multilayered aquifer in Lower Kelantan Basin, Kelantan, Malaysia *Environ. Earth Sci.* **77** 1–15
- Sestini G 1989 Nile Delta: a review of depositional environments and geological history *Geol. Soc. London Spec. Publ.* **41** 99–127
- Seto K C 2011 Exploring the dynamics of migration to mega-delta cities in Asia and Africa: contemporary drivers and future scenarios *Glob. Environ. Change* **21** S94–S107
- Shamsudduha M, Taylor R G, Ahmed K M and Zahid A 2011 The impact of intensive groundwater abstraction on recharge to a shallow regional aquifer system: evidence from Bangladesh *Hydrogeol. J.* **19** 901–16
- Shamsudduha M and Uddin A 2007 Quaternary shoreline shifting and hydrogeologic influence on the distribution of groundwater arsenic in aquifers of the Bengal Basin *J. Asian Earth Sci.* **31** 177–94
- Shi L and Jiao J J 2014 Seawater intrusion and coastal aquifer management in China: a review *Environ. Earth Sci.* **72** 2811–9
- Shi X, Fang R, Wu J, Xu H, Sun Y Y and Yu J 2012 Sustainable development and utilization of groundwater resources considering land subsidence in Suzhou, China *Eng. Geol.* **124** 77–89
- Simachaya W, Watanamahart P, Kaewkrajang V and Yenpiem A 2000 Water quality situation in the Chao Phraya Delta *Proc. Int. Conf.: The Chao Phraya Delta: Historical Development, Dynamics and Challenges of Thailand's Rice Bowl* pp 1–21
- Simpson G and Hutcheon I 1995 Pore-water chemistry and diagenesis of the modern Fraser River delta *J. Sediment. Res.* **65A** 648–55
- Sinsakul S 2000 Late Quaternary geology of the Lower Central Plain, Thailand *J. Asian Earth Sci.* **18** 415–26
- Smajgl A, Toan T Q, Nhan D K, Ward J, Trung N H, Tri L Q, Tri V P D and Vu P T 2015 Responding to rising sea levels in the Mekong Delta *Nat. Clim. Change* **5** 167–74
- Spratt R M and Lisiecki L E 2016 A Late Pleistocene sea level stack *Clim. Past* **12** 1079–92
- Stanley D J and Warne A G 1993 Nile Delta: recent geological evolution and human impact *Science* **260** 628–34
- Stanley D J and Warne A G 1994 Worldwide initiation of Holocene marine deltas by deceleration of sea-level rise *Science* **265** 228–31
- Stanton J S *et al* 2017 *Brackish Groundwater in the United States* 1833 USGS (<https://doi.org/10.3133/pp1833>)

- Stoecker F, Babel M S, Gupta A D, Rivas A A, Evers M, Kazama F and Nakamura T 2013 Hydrogeochemical and isotopic characterization of groundwater salinization in the Bangkok aquifer system, Thailand *Environ. Earth Sci.* **68** 749–63
- Stuyfzand P J 1997 Patterns in ground water chemistry resulting from ground water flow *Hydrogeol. J.* **7** 15–27
- Stuyfzand P J and Stuurman R J 2006 Origin, distribution and chemical mass balances of non-anthropogenic, brackish and (hyper) saline groundwaters in the Netherlands *Proc. 1st SWIM-SWICA Joint Saltwater Intrusion Conf. (Cagliari, Italy, 24–29 September 2006)* ed G Barrocu pp 151–64
- Surfsara 2014 *Surfsara Userinfo* (available at: <https://userinfo.surfsara.nl/systems/cartesius/description>) (Accessed 14 May 2018)
- Sutanudjaja E H et al 2018 PCR-GLOBWB 2: a 5 arcmin global hydrological and water resources model *Geosci. Model Dev.* **11** 2429–53
- Switzman H, Coulibaly P and Adeel Z 2015 Modeling the impacts of dryland agricultural reclamation on groundwater resources in northern Egypt using sparse data *J. Hydrol.* **520** 420–38
- Syvitski J P M et al 2009 Sinking deltas due to human activities *Nat. Geosci.* **2** 681–6
- Syvitski J P and Saito Y 2007 Morphodynamics of deltas under the influence of humans *Glob. Planet. Change* **57** 261–82
- Talukder M R R, Rutherford S, Huang C, Phung D, Islam M Z and Chu C 2017 Drinking water salinity and risk of hypertension: a systematic review and meta-analysis *Arch. Environ. Occup. Health* **72** 126–38
- Tamura T, Saito Y, Sieng S, Ben B, Kong M, Sim I, Choup S and Akiba F 2009 Initiation of the Mekong River delta at 8 ka: evidence from the sedimentary succession in the Cambodian lowland *Quat. Sci. Rev.* **28** 327–44
- Tanabe S, Saito Y, Lan Vu Q, Hanebuth T J, Lan Ngo Q and Kitamura A 2006 Holocene evolution of the Song Hong (Red River) delta system, northern Vietnam *Sediment. Geol.* **187** 29–61
- Teatini P, Ferronato M, Gambolati G and Gonella M 2006 Groundwater pumping and land subsidence in the Emilia-Romagna coastland, Italy: modeling the past occurrence and the future trend *Water Resour. Res.* **42** 1–19
- Teatini P, Tosi L, Vezzoli A, Baradello L, Zecchin M and Silvestri S 2011 Understanding the hydrogeology of the Venice Lagoon subsurface with airborne electromagnetics *J. Hydrol.* **411** 342–54
- Tessler Z, Vorosmarty C, Grossberg M, Gladkova I, Aizenman H, Syvitski J P M and Foufala-Georgiou E 2015 Profiling risk and sustainability in coastal deltas of the world *Science* **349** 638–43
- Thompson C, Smith L and Maji R 2007 Hydrogeological modeling of submarine groundwater discharge on the continental shelf of Louisiana *J. Geophys. Res.: Oceans* **112** 1–13
- Tilmans W M 1991 Coast erosion management—the Kelantan case *Ocean Shoreline Manage.* **15** 87–124
- Törnqvist T E, Wortman S R, Mateo Z R P, Milne G A and Swenson J B 2006 Did the last sea level lowstand always lead to cross-shelf valley formation and source-to-sink sediment flux? *J. Geophys. Res.: Earth Surf.* **111** 1–13
- Tran D A, Tsujimura M, Vo L P, Nguyen V T, Kambuku D and Dang T D 2019 Hydrogeochemical characteristics of a multi-layered coastal aquifer system in the Mekong Delta, Vietnam *Environ. Geochem. Health* **42** 661–80
- Tran L T, Larsen F, Pham N Q, Christiansen A V, Tran N, Vu H V, Tran L V, Hoang H V and Hinsby K 2012 Origin and extent of fresh groundwater, salty paleowaters and recent saltwater intrusions in Red River flood plain aquifers, Vietnam *Hydrogeol. J.* **20** 1295–313
- Van Driel W et al 2015 Vulnerability assessment of deltas in transboundary river basins *Technical Report* (Delft: Delta Alliance International)
- van Engelen J 2022 delta\_aquifer v0.2 (Zenodo) (<https://doi.org/10.5281/zenodo.6350503>)
- van Engelen J, Bierkens M F, Delsman J R and Oude Essink G H 2020 Factors determining the natural fresh-salt groundwater distribution in deltas *Water Resour. Res.* **57** e2020WR027290
- van Engelen J, Verkaik J, King J, Nofal E R, Bierkens M F P and Oude Essink G H P 2019 A three-dimensional palaeohydrogeological reconstruction of the groundwater salinity distribution in the Nile Delta Aquifer *Hydrol. Earth Syst. Sci.* **23** 5175–98
- Van Pham H, van Geer F C, Tran V B, Dubelaar W and Oude Essink G H 2019 Paleo-hydrogeological reconstruction of the fresh-saline groundwater distribution in the Vietnamese Mekong Delta since the late Pleistocene *J. Hydrol.: Reg. Stud.* **23** 1–22
- Verkaik J, van Engelen J, Huizer S, Bierkens M F, Lin H X and Oude Essink G H 2021 Distributed memory parallel computing of three-dimensional variable-density groundwater flow and salt transport *Adv. Water Resour.* **154** 103976
- Wang Y and Jiao J J 2012 Origin of groundwater salinity and hydrogeochemical processes in the confined Quaternary aquifer of the Pearl River Delta, China *J. Hydrol.* **438–439** 112–24
- Weatherall P, Marks K M, Jakobsson M, Schmitt T, Tani S, Arndt J E, Rovere M, Chayes D, Ferrini V and Wigley R 2015 A new digital bathymetric model of the world's oceans *Earth Space Sci.* **2** 331–45
- Werner A D, Bakker M, Post V E A, Vandenbohede A, Lu C, Ataie-Ashtiani B, Simmons C T and Barry D A 2013 Seawater intrusion processes, investigation and management: Recent advances and future challenges *Adv. Water Resour.* **51** 3–26
- Winkel L H E, Pham T K T, Vi M L, Stengel C, Amini M, Nguyen T H, Pham H V and Berg M 2011 Arsenic pollution of groundwater in Vietnam exacerbated by deep aquifer exploitation for more than a century *Proc. Natl Acad. Sci. USA* **108** 1246–51
- Wittmeyer G, Miklas M, Klar R, Williams D and Balin D 1996 Use of groundwater in the arid and semi-arid Western United States: implications for Yucca Mountain area *Technical Report NRC-02-93-005* (San Antonio, TX: Center for Nuclear Waste Regulatory Analyses)
- Wolters M L and Kuenzer C 2015 Vulnerability assessments of coastal river deltas—categorization and review *J. Coast. Conserv.* **19** 345–68
- Wu H and Zhu J 2010 Advection scheme with 3rd high-order spatial interpolation at the middle temporal level and its application to saltwater intrusion in the Changjiang Estuary *Ocean Modelling* **33** 33–51
- Xue Y Q, Wu J C, Zhang Y, Ye S J, Shi X Q, Wei Z X, Li Q F and Yu J 2008 Simulation of regional land subsidence in the southern Yangtze Delta *Sci. China D* **51** 808–25
- Yamanaka T, Shimada J, Tsujimura M, Lorphensri O, Mikita M, Hagihara A and Onodera S 2011 Tracing a confined groundwater flow system under the pressure of excessive groundwater use in the lower central plain, Thailand *Hydrol. Process.* **25** 2654–64
- Yang J, Graf T, Herold M and Ptak T 2013 Modelling the effects of tides and storm surges on coastal aquifers using a coupled surface-subsurface approach *J. Contam. Hydrol.* **149** 61–75
- Zamsky D, Essink G H, Sutanudjaja E H, Van Beek L P and Bierkens M F 2022 Offshore fresh groundwater in coastal unconsolidated sediment systems as a potential fresh water source in the 21st century *Environ. Res. Lett.* **17** 014021
- Zamsky D, Karssenberg M E, Cohen K M, Bierkens M F P, Gualbert H P and Essink O 2020 Geological heterogeneity of coastal unconsolidated groundwater systems worldwide and its influence on offshore fresh groundwater occurrence *Front. Earth Sci.* **7** 339

- Zamrsky D, Oude Essink G H and Bierkens M F 2018 Estimating the thickness of unconsolidated coastal aquifers along the global coastline *Earth Syst. Sci. Data* **10** 1591–603
- Zech A, Attinger S, Cvetkovic V, Dagan G, Dietrich P, Fiori A, Rubin Y and Teutsch G 2015 Is unique scaling of aquifer macrodispersivity supported by field data? *Water Resour. Res.* **51** 7662–79
- Zhang W, Feng H, Zheng J, Hoitink A, van der Vegt M, Zhu Y and Cai H 2013 Numerical simulation and analysis of saltwater intrusion lengths in the Pearl River Delta, China *J. Coast. Res.* **287** 372–82
- Zhou Q, Bear J and Bensabat J 2005 Saltwater upconing and decay beneath a well pumping above an interface zone *Transp. Porous Media* **61** 337–63
- Zong Y, Huang G, Switzer A D, Yu F and Yim W W 2009 An evolutionary model for the Holocene formation of the Pearl River delta, China *Holocene* **19** 129–42
- Zong Y, Huang K, Yu F, Zheng Z, Switzer A, Huang G, Wang N and Tang M 2012 The role of sea-level rise, monsoonal discharge and the palaeo-landscape in the early Holocene evolution of the Pearl River delta, southern China *Quat. Sci. Rev.* **54** 77–88